Progressive groundwater decoupling may drive a shift toward shallower and faster terrestrial water cycling

Aoqi Sun[1]†, Wenjie Xu[1]†, Enze Ma[2], Hua Yuan[1], Chen Yang[1]*

1 School of Atmospheric Sciences, Sun Yat-sen University, Zhuhai, China

2 College of Soil and Water Conservation Science and Engineering, Northwest A&F University, Yangling, China

†These authors contributed equally to this work

*Corresponding to: yangch329@mail.sysu.edu.cn

Abstract

Groundwater is widely regarded as a critical buffer that sustains evapotranspiration (ET) and streamflow under hydrologic stress. However, whether this buffering capacity persists under sustained increases in ET demand remains unclear. Here we test whether sustained increases in ET demand can reorganize subsurface connectivity and undermine effective groundwater buffering, using controlled hillslope simulations with integrated hydrologic modeling and particle tracking. Under baseline semi-arid forcing, ET and outflow exhibit coexisting young and older age components. Following late-summer groundwater drawdown, intermediate-age flow paths weaken, eventually producing a temporary age gap that separates shallow and deep sources. Outflow responds more abruptly than ET due to hydraulic disconnection at the outlet. Warming and vegetation greening amplify this intrinsic seasonal tendency. Intermediate-age contributions collapse earlier and recover more slowly, amplifying the polarization between shallow and deep water pools and further suppressing older groundwater inputs. Outflow becomes increasingly dominated by very young water, indicating strengthened groundwater–surface decoupling. These results suggest that sustained hydrologic stress structurally reduces effective groundwater connectivity, weakening subsurface buffering and shortening hydrologic memory. This tendency persists across parameter perturbations. As a consequence, water cycling shifts toward shallower and faster pathways. Progressive groundwater decoupling therefore represents not merely a change in source depth, but a structural transition toward a more rapidly recycled and potentially less predictable mode of terrestrial water cycling under sustained increases in terrestrial water use.

Deleted: Streamflow

Deleted: Stream

Formatted: Font color: Text 1

Formatted: Font color: Text 1

1. Introduction

Many terrestrial systems are increasingly exposed to hydrologic stress as atmospheric evaporative demand intensifies and biological water use expands. In this context, warming and vegetation enhancement act to amplify evapotranspiration (ET), increasing subsurface water extraction and tightening constraints on groundwater storage.

Groundwater is widely regarded as a critical buffer against such hydrologic stress (Condon et al., 2020; Miguez-Macho & Fan, 2025). Recent studies increasingly challenge the traditional separation of surface water and groundwater, arguing that they form a connected hydrologic continuum rather than two independent "water worlds" (Berkowitz & Zehe, 2020; Schiavo et al., 2022). By acting as a long-term storage reservoir and maintaining hydraulic connectivity with the shallow subsurface, groundwater regulates the timing and magnitude of surface water fluxes (Tran et al., 2020; Villaruel et al., 2025; Xie et al., 2024; Zipper et al., 2024), sustains ET and streamflow during dry periods (Betterle & Bellin, 2024; Knighton & Berghuijs, 2023), and provides hydrologic "memory" to the land surface system (Bierkens & van den Hurk, 2007; Brooks et al., 2021; Getirana et al., 2025; Liang et al., 2021). Under this prevailing view, drought is interpreted as a progressive shift toward deeper groundwater reliance: as shallow soil moisture is depleted, the relative contribution of groundwater increases, leading to older water signatures in both ET and streamflow due to the growing dominance of longer-residence subsurface water (Li et al., 2024; Swenson et al., 2024; Visser et al., 2019; C. Yang et al., 2023; X. Yang et al., 2021). Implicit in this interpretation is the tendency to assume that groundwater buffering remains effective even under sustained and intensifying hydrologic stress.

Carroll et al. (2024) examined how sustained warming alters groundwater–stream interactions using a high-resolution, observation-constrained integrated hydrologic model. Their simulations indicate that progressive groundwater storage decline lowers regional water tables and weakens hydraulic gradients toward stream channels, with some reaches shifting from historically groundwater-gaining to losing or weakly connected states during low-flow periods. Similarly, Betterle and Bellin (2024) showed that declining recharge lowers water tables and reduces subsurface storage. Under these conditions, the fraction of baseflow generated by groundwater increases, while the permanently active drainage network shrinks and shifts downstream, further reducing surface drainage density. In a drought-focused ecohydrological study, X. Yang et al. (2021) reported that transpiration could initially be maintained during the early stages of drought despite increasing water age, but declined sharply as drought conditions intensified, while evaporation remained comparatively stable. Collectively, these studies suggest that hydrologic responses to sustained stress may not be gradual, but instead involve substantial reorganization of groundwater connectivity, drainage networks, and vegetation water use.

In other words, these studies indicate that sustained hydrologic stress may alter not only the magnitude of water fluxes, but also the depth and pace at which water circulates through terrestrial systems. Rather than supporting the prevailing expectation that intensifying drought progressively increases groundwater dependence and shifts fluxes toward older water, these findings imply a different tendency: prolonged stress may reduce the effective contribution of deeper storage and favor younger, more rapidly recycled water sources. **This possibility raises a broader and largely**

Deleted: (Berkowitz & Zehe, 2020; Schiavo et al., 2022)G

Deleted: contributions

Formatted: Font color: Text 1

Deleted: Using a high-resolution, observation-constrained integrated hydrologic model of the East River headwaters in the Upper Colorado River basin,

Deleted: in a snow-dominated mountain system

Deleted: These results suggest that sustained climatic stress may reorganize groundwater–surface water exchange regimes.

Formatted: Font: (Default) Times New Roman, (Asian) Times New Roman

Formatted: Font: (Default) Times New Roman, (Asian) Times New Roman

Deleted: Similarly, Knighton and Berghuijs (2023), in a large-sample analysis of 472 U.S. watersheds, linked ET water age to long-term ET magnitude and ecosystem drought resilience. Watersheds characterized by older ET water tended to exhibit higher long-term ET but slower post-drought recovery, whereas systems dominated by younger ET water showed greater resilience. While focused on watershed-scale ET age rather than groundwater connectivity, these findings indicate that water age metrics capture structural aspects of ecosystem water use under stress. ¶
Taken together

Deleted: Carroll et al. (2024)Betterle and Bellin (2024)X. Yang et al. (2021)The East River simulations demonstrate that groundwater storage decline can weaken deep groundwater contributions to streams, while the large-sample analysis of ET water age suggests that reliance on older water is not necessarily enhanced under stress and may instead be associated with reduced resilience.

Deleted: strengthens

Deleted: buffering

Deleted: progressively

unresolved question: can sustained hydrologic stress shift terrestrial water cycling toward a shallower and faster regime, rather than simply intensifying groundwater dependence?

Here we hypothesize that persistent increases in ET demand may shift terrestrial water cycling toward shallower and faster pathways, manifested through a systematic reorganization of internal water age structure. As groundwater storage declines beyond a critical threshold, intermediate-age contributions may collapse, leading to a separation between shallow, rapidly recycled water and deeper, longer-residence storage (**Figure 1**). This age polarization reflects a weakening of hydraulic connectivity between deep and shallow domains and signals a shift from a coupled regime—where multiple storage pools jointly regulate surface fluxes—to a decoupled regime dominated by shallower and faster flow paths. Here, reorganization refers to this structural redistribution of water-age contributions driven by changing subsurface connectivity, including the contraction or loss of intermediate flow paths rather than a simple shift in the relative magnitude of existing contributions.

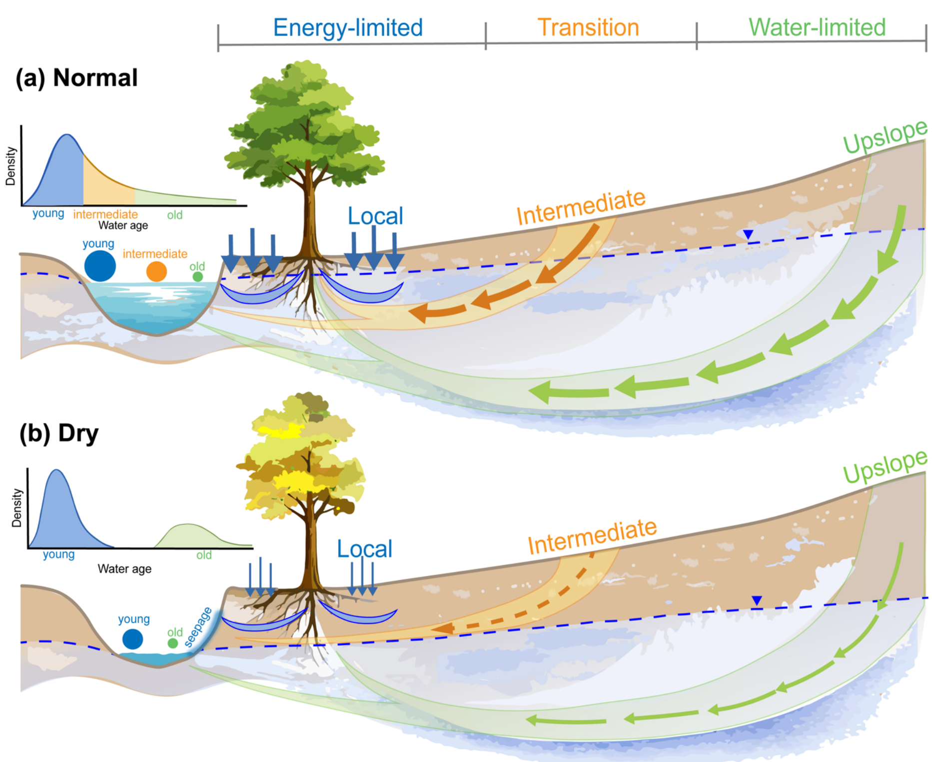

Figure 1. Shift from coupled to segregated flow structure with age polarization under groundwater decline. (a) Under wetter conditions, shallow, intermediate, and deep flow

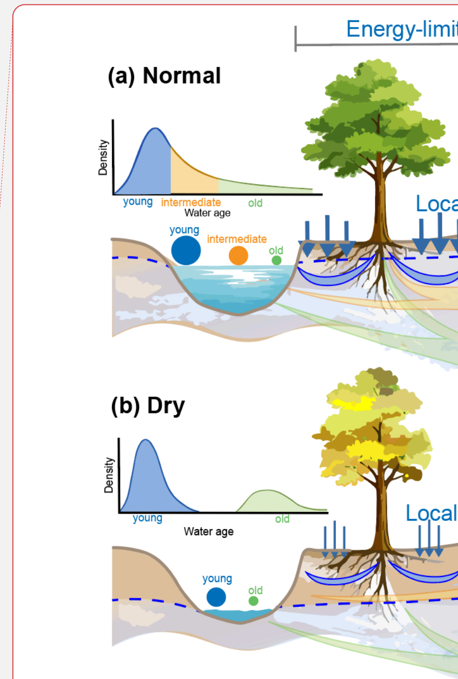

Deleted:

Formatted: Font color: Text 1

Formatted: Font color: Text 1

Deleted: Figure 1. Shift from coupled to segregated flow structure with age polarization under groundwater decline. Arrows illustrate dominant source regions rather than exact flow trajectories

Formatted: Font: Bold, Font color: Text 1

paths jointly contribute to ET and streamflow. (b) Under drier conditions, weakening hydraulic connectivity suppresses intermediate-age contributions, producing age segregation between young local water and older deep storage. Arrows illustrate dominant source regions rather than exact flow trajectories.

To examine this possibility, we design a set of controlled hillslope experiments that systematically increase ET forcing and track the resulting evolution of water storage partitioning and water age structure. The hillslope represents the fundamental hydrologic unit (Fan et al., 2019) where vertical and lateral processes interact, and subsurface flow organization is most directly expressed. This framework allows ET and streamflow age dynamics to be interpreted jointly within a common hillslope-scale context. The controlled configuration enables clear diagnosis of mechanism, providing a baseline understanding that can inform interpretation of more complex real-world systems where multiple interacting processes operate simultaneously.

2. Methods

To examine how enhanced ET forcing influences subsurface storage partitioning and internal water age distribution, we conducted controlled numerical experiments in a synthetic quasi-three-dimensional domain (Bearup et al., 2016; Danesh-Yazdi et al., 2018; Mikkelson et al., 2013). The domain represents a 100 m long, 1 m wide, and 9.4 m deep hillslope with a uniform surface gradient of 0.1 (**Figure S3**). The hillslope was discretized using a terrain-following grid (Maxwell, 2013) at 5 m resolution along-slope and 0.2 m across-slope, with 20 vertical layers of variable thickness: 0.5 m in the deeper subsurface, gradually refining to 0.3 m and 0.1 m near the surface to better resolve shallow processes. The upper 10 layers (4.4 m) constitute the root zone, where ParFlow and CLM exchange water fluxes. Subsurface hydraulic properties were specified uniformly. Saturated hydraulic conductivity was set to 0.05 m h^{-1}, porosity to 0.20, and van Genuchten parameters to $\alpha = 1.0$ m^{-1} and $n = 2$, and residual saturation (S_{res}) to 0.2. These hydraulic properties were adopted from previous ParFlow–EcoSLIM studies (Maxwell et al., 2019; Yang et al., 2022). Together with the prescribed tree-covered vegetation, these parameter values are broadly representative of semi-arid woody hillslopes commonly characterized by shallow soils, weathered bedrock, and limited subsurface water storage. This configuration serves as the reference state for subsequent perturbation experiments.

Water fluxes were simulated using the integrated hydrologic model ParFlow–CLM (Kollet & Maxwell, 2006, 2008; Maxwell & Miller, 2005), which resolves coupled land surface processes and variably saturated subsurface flow with lateral groundwater dynamics. The governing equations of ParFlow–CLM and the particle-tracking formulation used in EcoSLIM are summarized in Text S1 of the Supplementary Information. The system was forced with a representative semi-arid meteorological record from the Little Washita watershed in Oklahoma (USA), providing realistic atmospheric demand and precipitation variability for a water-limited hillslope environment (Kollet & Maxwell, 2008; Maxwell et al., 2019). The model was spun up for three years, and the third-year state was used to initiate particle tracking. EcoSLIM (Maxwell et al., 2019; Yang et al., 2022; C. Yang et al., 2021) simulations were then conducted for 20 years to allow age distributions to approach dynamic equilibrium. All ParFlow–CLM and EcoSLIM simulations were performed with an hourly time step.

Moved down [2]: The hillslope represents the fundamental hydrologic unit (Fan et al., 2019) where vertical and lateral processes interact, and subsurface flow organization is most directly expressed.

Moved (insertion) [2]

Deleted: By isolating this elementary unit under realistic meteorological forcing, we focus on diagnosing the intrinsic reorganization of age-structured water cycling under increasing ET demand. This controlled configuration enables clear diagnosis of mechanism, providing a baseline understanding that can inform interpretation of more complex real-world systems where multiple interacting processes operate simultaneously.

Field Code Changed

Formatted: Font color: Text 1

Formatted: Font color: Text 1

Deleted: Although resolved in three dimensions, the narrow across-slope width emphasizes dominant along-slope subsurface flow and lateral groundwater dynamics. ¶

Deleted: ~~The land surface was prescribed as tree-covered vegetation representative of semi-arid woody hillslopes.~~

Deleted: This configuration enables explicit representation of vegetation uptake and shallow soil moisture dynamics, while maintaining fully coupled groundwater flow beneath. ¶

Moved down [1]: (Maxwell et al., 2019; Yang et al., 2022)

Deleted: These geometric and hydraulic specifications define a physically consistent semi-arid hillslope suitable for examining structural shifts in subsurface water cycling under controlled forcing.

Deleted: (Maxwell et al., 2019; Yang et al., 2022)

Deleted: characteristic of

EcoSLIM uses the transient flow fields and ET fluxes generated by ParFlow–CLM to simulate particle advection and molecular diffusion, thereby explicitly tracking the transport pathways and residence times of water within the coupled land–groundwater system. Diagnostics were derived from the twentieth year. During the final analysis year, the domain consistently contained on the order of 10^6 actively circulating particles. Over the course of that year, 2.17×10^5 particles exited the domain as subsurface outflow and 2.48×10^5 were removed via ET. Because particle inflow and release were continuous, the in-domain particle population remained approximately constant while flux-specific particles were sampled as they exited. This high particle density and sustained turnover enable robust, high-resolution characterization of flux age structure under different ET forcing scenarios.

Building upon this baseline configuration, four primary forcing scenarios were constructed: a baseline case, a +1 °C warming perturbation, a 50% increase in maximum leaf area index (LAI), and a combined warming–greening scenario. The +1 °C warming perturbation represents a moderate future climate signal (Ipcc, 2021). The LAI perturbation magnitude reflects an enhanced yet plausible continuation of observed multi-decadal greening trends (Piao et al., 2020). Satellite observations indicate widespread increases in vegetation greenness globally, with particularly strong greening occurring in several hotspot regions (Chen et al., 2019). The imposed 50% increase in maximum LAI is therefore intended as an enhanced perturbation to explore the hydrologic consequences of sustained vegetation expansion rather than to reproduce a specific observed magnitude of change. Baseline and perturbed LAI values are summarized in Table S1.

Deleted: realistic

Deleted: ,

Deleted: while the +1 °C warming represents a moderate future climate signal (Ipcc, 2021).

To evaluate structural robustness, three additional experimental groups were conducted in which key system properties were modified relative to the reference parameter set. In the first group, vegetation type was changed from trees to shrubs, representing shallower rooting systems and reduced transpiration demand. In the second group, subsurface hydraulic parameters were adjusted, with saturated hydraulic conductivity set to 0.1 m h^{-1}, porosity to 0.39, van Genuchten parameters to α = 3.5 m^{-1} and n = 2, and S_{res} to 0.01 (Mikkelson et al., 2013), representing a transition from relatively low-porosity, semi-arid soils to more permeable, coarse-textured subsurface conditions. In the third group, hillslope gradient was reduced to 0.05, representing weaker topographic control on lateral drainage and groundwater convergence.

Table 1. Overview of the sixteen scenario combinations used in this study. Each row represents a distinct hillslope configuration, and each configuration was simulated under four ET-forcing scenarios.

Formatted: Justified

Formatted: Font: Bold

Configuraton	**Baseline**	**Warming**	**Greening**	**Warming+Greening**
Reference	✓	✓	✓	✓
Modified K	✓	✓	✓	✓
Modified Vegetation	✓	✓	✓	✓
Reduced Slope	✓	✓	✓	✓

Formatted: Left

Formatted Table

Formatted: Left

Formatted: Left

Formatted: Left

Formatted: Left

In total, four experimental groups comprising sixteen scenario combinations were simulated (Table 1), each employing particle tracking to characterize the evolution of subsurface water age structure. The objective of this experimental design is not to reproduce a specific field site or

Deleted: In total, four experimental groups comprising sixteen scenario combinations were simulated, each employing particle tracking to characterize the evolution of subsurface water age structure.

exhaustively sample parameter uncertainty, but rather to diagnose how key controls on terrestrial water cycling influence system behavior under increasing ET demand. Representative baseline values were therefore adopted and systematically perturbed to examine the direction and robustness of hydrologic responses across contrasting system configurations.

3. Results

3.1. Water fluxes

Under baseline conditions, seasonal water fluxes exhibit a pronounced late-summer transition governed by the interaction between groundwater storage and ET demand (**Figure 2**). Following gradual recovery during winter and spring, groundwater levels continue to rise and reach their shallowest condition between May and July (**Figure 2c**). Air temperature increases after early spring (**Figure S1**), and following a rainfall event in June, ET reaches its annual maximum in July (**Figure 2a**).

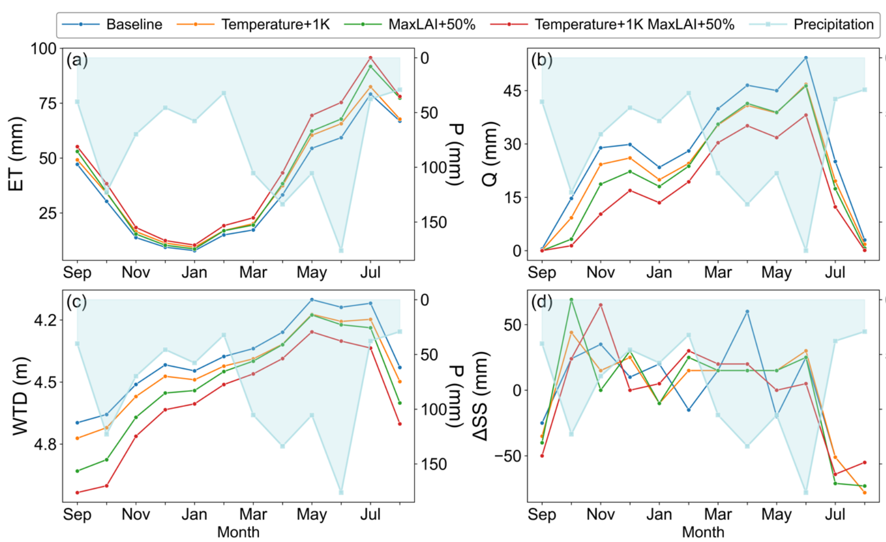

Figure 2. Seasonal evolution of water fluxes and states under baseline and enhanced ET-forcing scenarios. Panels show monthly mean (a) evapotranspiration (ET), (b) streamflow (Q), (c) water table depth (WTD), and (d) saturated storage change (ΔSS), calculated from hourly model outputs during the corresponding analysis year. Precipitation (P) is shown on the secondary axis in each panel. Enhanced ET forcing through warming (+1 °C), greening (MaxLAI+50%), and their combination amplifies seasonal groundwater depletion, resulting in deeper water tables and larger storage losses during the late growing season.

Moved (insertion) [3]

Deleted: Figure 2. Monthly precipitation (P), evapotranspiration (ET), streamflow (Q), water table depth (WTD), and saturated storage change (ΔSS) under baseline and enhanced ET forcing

Formatted: Font: Bold

Formatted: Font: Bold

Formatted: Font: Bold

Formatted: Font: Bold

The July ET peak triggers a rapid groundwater decline. With relatively modest rainfall in July and August, groundwater drawdown continues even though ET weakens slightly in August; ET remains substantial through August–September, pushing the water table to its annual maximum depth in September (deepest condition). Consistent with this progression, saturated storage shows pronounced net losses over July–September (**Figure 2d**), indicating that ET during this period is supported in part by groundwater withdrawal. Concurrently, the domain-averaged ET age increases (**Figure 3a**), consistent with greater reliance on older subsurface storage.

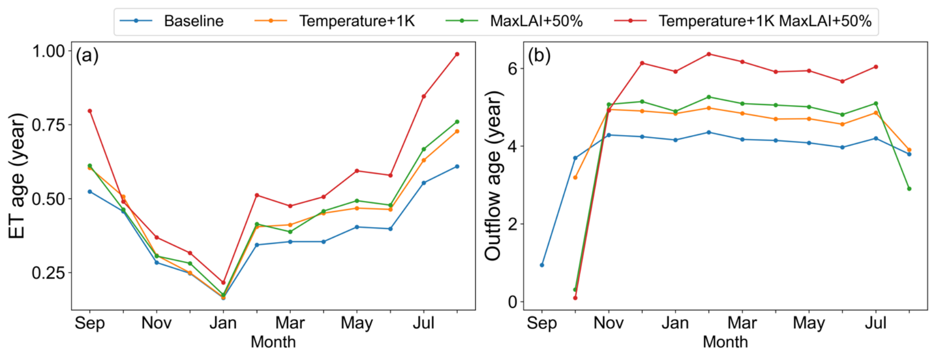

Figure 3. Monthly mean (a) ET age and (b) outflow age under baseline and enhanced ET-forcing scenarios. Values represent monthly averages calculated from hourly outputs during the corresponding analysis year. Missing outflow-age values indicate months with zero outflow, during which no outflow age could be computed. Enhanced ET forcing generally increases both ET and outflow ages and amplifies seasonal age contrasts, while periods of absent outflow reflect temporary groundwater–surface decoupling at the hillslope outlet.

After September, ET declines from late-summer levels (September) and continues decreasing through autumn (October–November), reaching a minimum in mid-winter (December–January), before gradually increasing again in late spring (April–May). Although precipitation remains moderate during autumn and winter (October–February), both atmospheric demand and vegetation activity are strongly reduced (**Figure S1**). Lower air temperature suppresses evaporative demand, while reduced LAI during the dormant season limits transpiration, jointly constraining ET. As a result, water inputs exceed atmospheric losses during this period, allowing groundwater storage to progressively recover from autumn through spring, with groundwater levels becoming shallow again by May.

Streamflow closely tracks seasonal groundwater dynamics (**Figure 2b**). Discharge reaches its annual maximum in June, when groundwater levels are shallow, and declines toward a minimum in September as the water table reaches its deepest condition. In contrast to the maximum ET age observed during late-summer groundwater drawdown, outflow age exhibits the opposite tendency during August–October, declining sharply as outflow becomes dominated by very young water (**Figure 3b**). This age decrease reflects hydraulic disconnection between the channel and deeper

Deleted: ¶
Figure 3. Monthly mean ET and outflow ages under different ET forcing scenarios¶

Formatted: Normal, Left, Level 3, Space Before: Auto, After: Auto

Formatted: Font: Bold

Formatted: Font: Bold

Formatted: Font: Bold

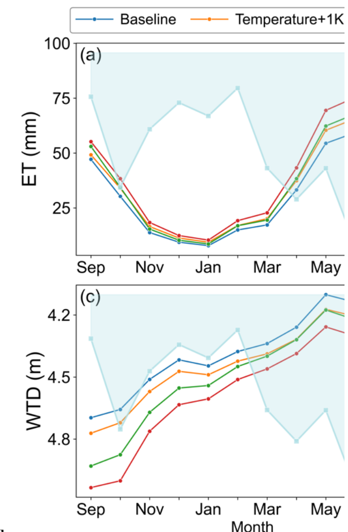

Moved up [3]:
Figure 2. Monthly precipitation (P), evapotranspiration (ET), streamflow (Q), water table depth (WTD), and saturated storage change (ΔSS) under baseline and enhanced ET forcing¶

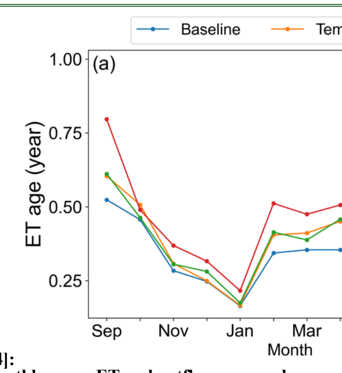

Moved up [4]:
Figure 3. Monthly mean ET and outflow ages under different ET forcing scenarios¶

Deleted: stream

groundwater once the water table drops below the outlet elevation (**Figure S2**), effectively suppressing older groundwater contributions.

In addition to the late-summer minimum in streamflow, two secondary discharge declines are evident (**Figure 2b**): one in January and another in May. The January dip reflects a delayed drainage adjustment following enhanced recharge and temporarily strengthened hydraulic connectivity in autumn. After the October rainfall temporarily increases subsurface water availability, the system undergoes accelerated drainage through November and December, progressively depleting stored water. By January, despite a modest precipitation peak, discharge declines because much of the transiently accumulated storage has already been drained (**Figure S3**). The May reduction, in contrast, corresponds to a sharp increase in ET relative to April. As atmospheric demand rises and vegetation activity resumes, increased ET suppresses groundwater discharge, producing a secondary decline before peak flow is reached in June.

Deleted: out

This seasonal transition sets the stage for the structural reorganization of internal water age described below.

3.2. Age distributions

Under baseline conditions, ET and outflow exhibit two persistent age components: young, locally recharged water and older groundwater-sourced water (**Figures 4–6 and S4–S6**). These components vary seasonally but generally coexist. Although ET ages are computed across the entire hillslope, the discussion below focuses on the downslope portion (approximately the lower 20 m). In this zone, soil saturation remains close to unity for much of the year (**Figure S3**), maintaining strong lateral convergence and vertical hydraulic connectivity across the profile. The shallow subsurface therefore remains well coupled to deeper groundwater storage, and water availability is rarely limiting. As a result, the ET age spectrum in this region reflects contributions from both locally recharged downslope water and older upslope groundwater storage.

Particle source diagnostics further confirm this spatial separation of age components. ET particles with ages between 0.5–1 year predominantly originate within the lower ~20 m of the hillslope, indicating a locally recharged downslope water source (**Figure S7**). In contrast, particles with ages between 1–2.5 years are traced to positions upslope of 20 m, demonstrating that older ET contributions are supplied by more distal upslope groundwater storage (**Figure S8**). This age-dependent upslope shift in source location confirms that the two age components correspond to locally recharged downslope water and older upslope groundwater storage.

Following the late-summer drying (around September), the water table deepens. As the system desaturates, intermediate subsurface flow paths that connect shallow storage to deeper groundwater weaken. In the subsequent months, ET remains at a moderate level and continues to draw partly on deeper soil water, so the intermediate-age component does not vanish immediately. However, as ET gradually decreases toward winter, its reliance on deeper water diminishes and the contribution of locally stored shallow water becomes more prominent. This seasonal shift in water use progressively reduces the relative contribution of older water in the ET age distribution, as reflected by the gradual fading of high-density colors in the older age range (**Figures 4 and 5**).

By January, when ET demand is minimal, water use is largely confined to shallow near-surface storage (**Figure S9**). Meanwhile, portions of the intermediate-age water stored in deeper soil layers were reduced during transient drainage in the preceding months, and the delayed drying signal from upslope areas has propagated downslope. The combined effect of prior drainage and delayed signal transmission results in a temporary loss of intermediate-age contributions, producing the pronounced age gap observed in early winter (January, **Figures 4 and 5**). Here, the term *age gap* refers to a marked depletion of intermediate-age contributions that separates younger and older water components within the age distribution. Notably, this age-gap formation coincides with the January dip in streamflow (**Figure 2b**), indicating that the short-lived autumn recharge did not fully reverse the preceding drying signal.

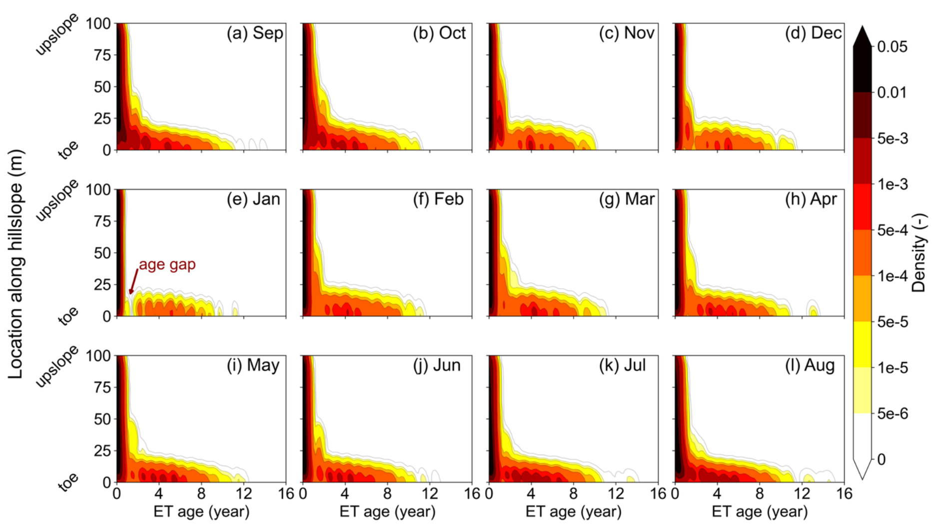

Figure 4. Monthly spatial distribution of ET age along the hillslope under baseline conditions. The vertical axis represents *x*-location along the hillslope, with 0 m corresponding to the hillslope toe and 100 m to the upslope boundary. Colors indicate the probability density of ET ages. Under baseline conditions, ET age distributions evolve seasonally from a relatively continuous age structure in autumn to a pronounced depletion of intermediate-age contributions in winter (January), producing a temporary age gap that separates younger and older water components before reconnecting during the subsequent recovery period.

Formatted: Font: Italic

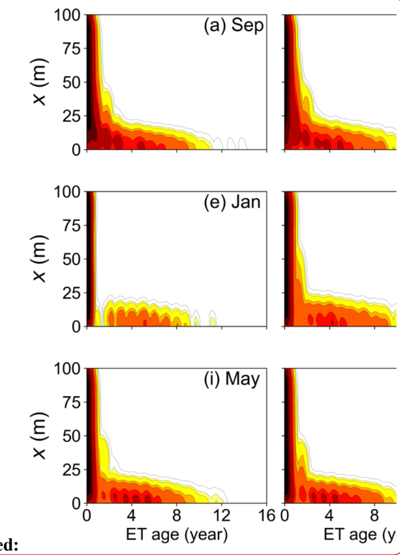

Deleted:

Deleted: Figure 4. Monthly spatial distribution of ET age along the hillslope under baseline conditions

Formatted: Font: Italic

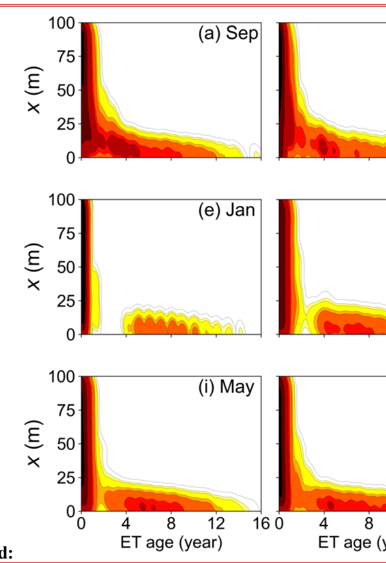

Deleted:

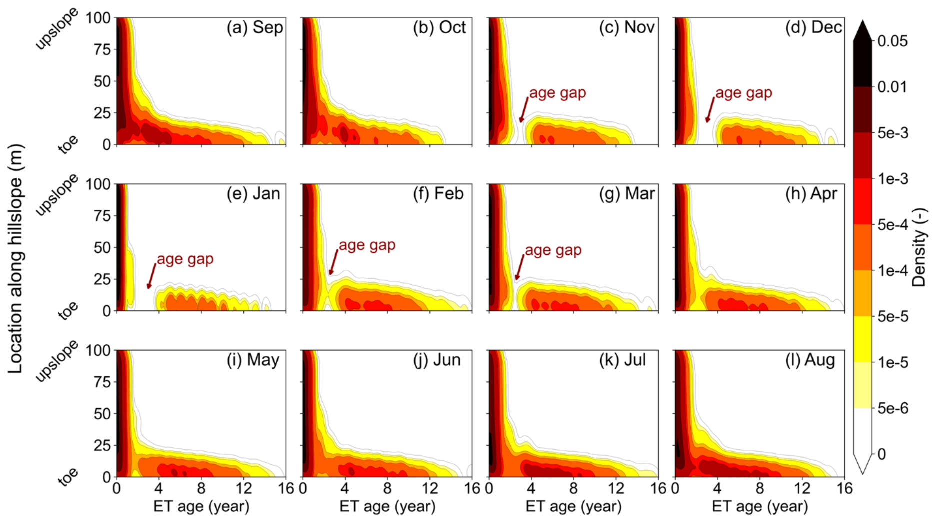

Figure 5. Monthly spatial distribution of ET age along the hillslope under combined warming–greening forcing. Colors indicate the probability density of ET ages. Compared with the baseline case (Figure 4), enhanced ET forcing promotes earlier and more pronounced depletion of intermediate-age contributions, resulting in a larger and more persistent age gap and stronger separation between young and old water components.

Particle source diagnostics (**Figure 7**) reveal two spatially distinct ET source regions, with contributions originating from both proximal downslope storage and more distal upslope portions of the hillslope. Following late-summer depletion, contributions from the slope segment immediately upslope of the lower 20 m zone are markedly reduced. This segment corresponds to the transition from energy-limited to water-limited conditions (**Figure S10**) and represents a key bridging pathway linking deeper upslope storage to downslope ET (**Figure 1**). ET increases markedly along the downslope transition zone (approximately 20–60 m), particularly during July–September (**Figure S10**). However, soil saturation in this region does not reach the more favorable moisture conditions observed at the hillslope toe (lower 20 m, **Figure S3**), rendering it more vulnerable to moisture limitation during dry or drought periods. This vulnerability likely disrupts intermediate subsurface flow paths, contributing to the observed contraction of bridging connectivity and the emergence of the ET age gap.

Outflow responds more abruptly than ET. In September, groundwater levels reach their annual minimum, and at the hillslope outlet the water table drops below the land surface elevation, effectively disconnecting deeper groundwater from the channel. As a result, older groundwater contributions rapidly diminish, leaving outflow dominated by very young, locally recharged water generated primarily through saturation-excess runoff (**Figure 6a**).

Deleted: Figure 5. Monthly spatial distribution of ET age along the hillslope under combined warming–greening forcing…

Deleted: Streamflow

Deleted: streamflow

As precipitation increases in October, older groundwater contributions begin to reappear at the outlet. However, this re-emergence remains separated from the young component by a pronounced age gap, reflecting the incomplete recovery of intermediate-age contributions (**Figure 6a**). Unlike ET, which can actively tap locally stored deeper soil water through root uptake and thus temporarily retain intermediate-age contributions, outflow behaves as a passive drainage flux. Once hydraulic connectivity weakens, intermediate-age contributions decline immediately and remain suppressed until subsurface connectivity is progressively restored through seasonal recharge.

By mid-winter (January–February), the earlier drying signal has largely drained through the system, while concurrent recharge gradually rebuilds storage (**Figure 6a**). Consequently, the age gap narrows progressively through late winter and spring, signaling the seasonal reactivation of intermediate pathways and the gradual restoration of subsurface connectivity.

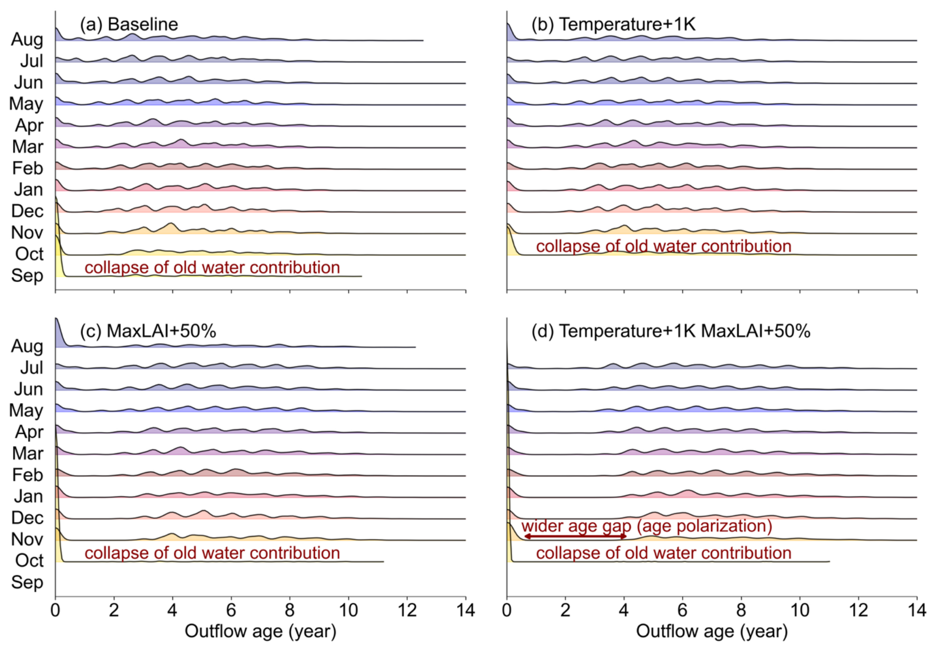

Figure 6. Monthly outflow age distributions under four ET-forcing scenarios: (a) baseline, (b) warming (+1 °C), (c) greening (MaxLAI +50%), and (d) combined warming–greening forcing. The horizontal axis shows outflow age, and the vertical axis represents individual months from September to August. Each ridge corresponds to the probability density distribution of outflow ages for a given month. Under baseline conditions, the older-age component temporarily disappears in September. Under the enhanced ET-forcing scenarios, a similar collapse occurs in October. Enhanced ET forcing also produces a wider separation

Deleted: streamflow

Deleted: ¶

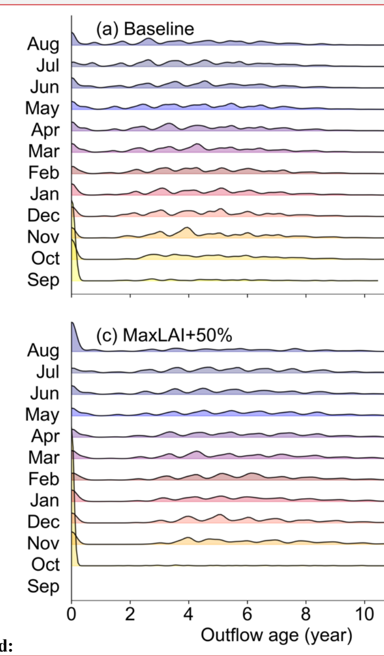

Deleted:

Deleted: Figure 6. Monthly outflow age distributions under four ET forcing scenarios

Formatted: Justified

between younger and older age components, resulting in a more pronounced age gap and stronger age polarization under the combined warming–greening scenario.

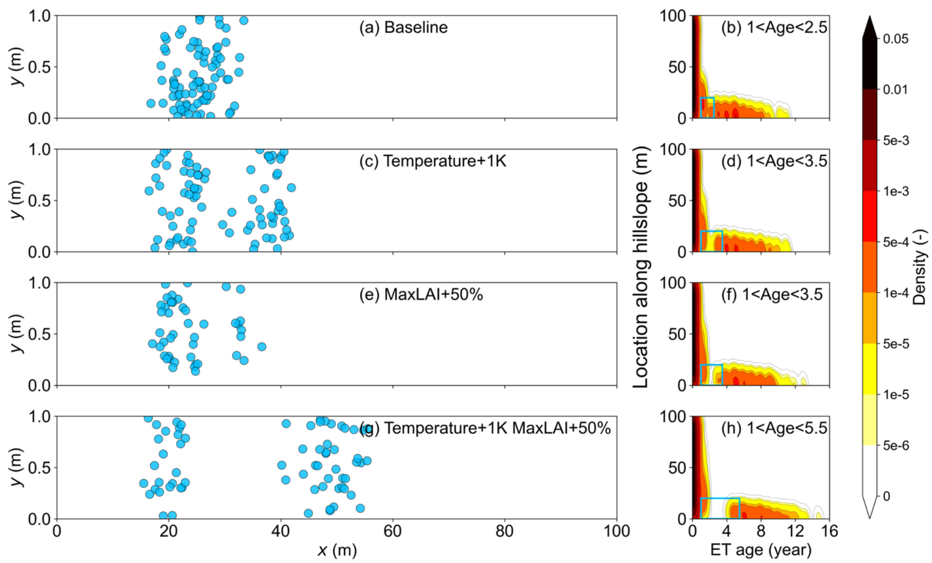

Figure 7. Source regions of particles contributing to December ET in the lower 20 m zone of the hillslope for selected age ranges under different ET-forcing scenarios. Left panels show the inferred source locations of these ET-contributing particles in the x–y domain, where x represents distance along the hillslope and y represents the across-slope direction. Right panels show the corresponding ET age distributions as a function of distance along the hillslope, with the same x coordinate shown on the vertical axis. Blue rectangles indicate the selected age intervals used to identify the particle populations shown in the left panels.

3.3. Warming and greening

Warming and vegetation greening both intensify this seasonal reorganization of ET age structure. Under these scenarios, intermediate-age contributions collapse more abruptly during late summer, so that a clear age gap emerges earlier than in the baseline case and remains prominent through the subsequent months (**Figures S4–S5**). The combined warming–greening scenario shows the strongest amplification: a distinct separation between shallow and deep age components is already evident by November, and the two components remain largely disconnected through winter and spring. Only by the following May does a weak partial reconnection begin to appear, indicating a delayed and incomplete return of intermediate-age contributions (**Figure 5**). Overall, enhanced ET forcing advances the onset of age segregation and prolongs the period over which ET draws from two separated shallow and deep source pools.

Deleted: ¶
Figure 7. Source regions of ET particles (lower 20 m zone) for selected age ranges under different ET forcing scenarios

Deleted: Figure 7. Source regions of ET particles (lower zone) for selected age ranges under different ET forcing scenarios

Deleted: ¶

Outflow exhibits an even more abrupt response under warming and greening (**Figures 6b–6d**). In September, discharge effectively collapses. Under the combined warming–greening scenario, October outflow is almost entirely composed of very young water, with older groundwater contributions nearly absent and a pronounced age gap separating the young and older components. Throughout the following months, the reconnection between young and older components remains weak. Even into early summer (around May), the restoration of intermediate-age connectivity remains incomplete, indicating a delayed and structurally weakened recovery of groundwater–surface water coupling.

Deleted: Stream

Importantly, these perturbations do not introduce a fundamentally new behavior, but amplify the intrinsic seasonal tendency toward groundwater–surface decoupling already present under baseline conditions. Warming and greening advance its onset, extend its duration, and in some cases push the system toward a quasi-persistent decoupled regime. In addition to advancing the onset of age segregation, warming and greening also enhance the polarization of the age spectrum, with young components becoming increasingly concentrated at very short residence times while older contributions are either shifted toward longer ages or temporarily suppressed. Taken together, these patterns indicate that progressive groundwater decoupling under enhanced ET forcing drives a shift toward faster and shallower terrestrial water cycling.

3.4 Structural robustness across parameter configurations

To evaluate whether the age-gap formation and deep–shallow decoupling depend on a specific parameter choice, we examined three additional parameter groups involving vegetation type, subsurface hydraulic properties, and hillslope gradient. Across all configurations, the qualitative reorganization pathway identified under the reference parameter configuration remains evident, although its magnitude varies. When vegetation was changed from trees to shrubs (**Figures S11–S12**), overall ET demand and seasonal water stress were reduced. As expected, both ET and outflow age structures became less polarized, and the seasonal age gap weakened, yet the separation between shallow and deep contributions remained discernible. This behavior is consistent with the stress-controlled nature of the mechanism: reduced water demand dampens, but does not eliminate, connectivity-driven reorganization.

Modifying subsurface hydraulic properties (**Figures S13–S14**) altered the balance of connectivity pathways without disrupting the underlying pattern. Higher saturated hydraulic conductivity and porosity enhanced lateral groundwater movement toward the hillslope toe, increasing the relative contribution of older groundwater to outflow. At the same time, larger α and lower residual saturation weakened capillary linkage between the root zone and deeper storage, reducing the older-water fraction in ET. As a result, outflow exhibited a greater proportion of old water, whereas ET shifted toward younger sources. In both fluxes, the age gap remained detectable but substantially muted, primarily reflecting a redistribution between young and old contributions. In contrast, reducing hillslope gradient (**Figures S15–S16**) weakened both lateral drainage and vertical hydraulic connectivity, amplifying seasonal decoupling. Under these conditions, old-water contributions nearly vanished during winter months in both ET and outflow, and the age gap became more pronounced during the rest of the year.

Together, these results indicate that parameter perturbations modulate the intensity and manifestation of groundwater–surface decoupling, but do not alter the underlying reorganization tendency. The emergence of age segregation under sustained stress therefore appears robust across variations in vegetation, hydraulic properties, and slope gradient.

4. Discussion

Fan et al. (2017) has emphasized that vegetation water use is regulated by two hydrologic regimes: shallow soil moisture supplied by rainfall infiltration and deeper groundwater accessible through hydraulic connectivity. Similarly, tracer studies show that streamflow integrates a fast, young-water regime and a slower, old-water regime linked to deeper storage (Floriancic et al., 2024). Our findings refine this dual-regime perspective by showing that under dry or drought conditions, declining hydraulic connectivity weakens the groundwater-controlled regime and may even lead to partial decoupling from deeper storage. Importantly, this mechanism does not contradict observations from many drought studies reporting an increase in the fraction of "old water" during dry periods (von Freyberg et al., 2018; Wilusz et al., 2019). Even when groundwater contributions diminish, source water ages may remain elevated because vegetation increasingly relies on water stored below the actively recycled shallow soil layer. Such water corresponds to deeper vadose-zone storage recharged by past infiltration events (Miguez-Macho & Fan, 2021), rather than groundwater stored below the water table. What we emphasize here is that increasing hydrologic stress does not necessarily lead to progressively greater dependence on the deepest groundwater reservoir; rather, its contribution may be suppressed as connectivity contracts (**Figure 1**). While derived from controlled hillslope experiments, the mechanism identified here isolates a fundamental reorganization pathway that may operate in real catchments under sustained stress.

Deleted: the relative importance of deeper soil moisture within the infiltration-controlled regime can increase, leading to slightly older effective source water

Deleted: What we emphasize here is that the deepest groundwater reservoir does not necessarily become progressively more engaged under increasing stress; rather, its contribution may be suppressed as connectivity contracts

The structural tendency identified here is unlikely to weaken under ongoing global change. Sustained warming and widespread vegetation greening increase atmospheric and biological water demand from above (Pokhrel et al., 2021; Y. Yang et al., 2023), while groundwater extraction reduces subsurface storage from below (Jasechko et al., 2024). These combined pressures intensify overall water stress and weaken deep–shallow hydraulic connectivity. The documented eastward shift of the hydroclimatic dry–wet boundary along the 100th meridian west in North America—reported to have migrated approximately 140 miles eastward since 1980 (Seager, Feldman, et al., 2018; Seager, Lis, et al., 2018)—suggests that an expanding fraction of landscapes is becoming increasingly water-limited, a condition under which subsurface connectivity is more prone to weakening. Recurrent groundwater drought and widespread baseflow decline further reflect this progressive loss of subsurface buffering (Elsaidy et al., 2025; Tan et al., 2020). Under such conditions, contraction of intermediate flow paths and groundwater–surface decoupling may become increasingly prevalent rather than exceptional.

A gradual loss of groundwater connectivity weakens the subsurface buffering capacity that stabilizes surface fluxes. As deep storage becomes less engaged, the hydrologic memory carried by long-residence water diminishes. Consequently, antecedent storage conditions exert a weaker influence on subsequent ET and streamflow, and fluxes become more directly controlled by short-term atmospheric forcing. With reduced temporal persistence, the capacity to infer future fluxes from present storage states declines. At the same time, the diminished participation of deep storage reduces the system's ability to absorb and moderate climatic extremes, weakening its resilience.

Such a system is therefore both more sensitive to external forcing and inherently more difficult to predict under sustained stress (Shi et al., 2022).

Although the additional parameter configurations examined here consistently preserved the underlying reorganization tendency, natural catchments involve simultaneous variations in vegetation, topography, subsurface properties, and climatic forcing. Interactions among these factors may amplify, suppress, or otherwise modify the manifestation of the mechanism identified in this study. In addition, several processes not explicitly represented here, including snow accumulation and melt, mountain-block recharge, and other forms of catchment heterogeneity, may alter the timing and magnitude of groundwater connectivity changes (Jencso et al., 2009; Somers & McKenzie, 2020). For example, seasonal snow storage can delay water release and sustain subsurface recharge during dry periods, potentially buffering the development of age segregation and deep–shallow decoupling. Future work is therefore needed to evaluate how the connectivity-driven reorganization identified here emerges in real catchments where multiple processes interact simultaneously.

Deleted: Future work will examine how this structural mechanism manifests in real catchments, where heterogeneity and multi-scale feedbacks interact with groundwater connectivity under complex climatic and geomorphic conditions.

5. Summary

This study demonstrates that sustained increases in ET demand may fundamentally reorganize the internal age structure of terrestrial water cycling. Using controlled hillslope experiments with integrated hydrologic modeling and particle tracking, we show that progressive groundwater storage decline weakens intermediate-age flow paths and separates shallow, rapidly recycled water from deeper, long-residence storage. Under enhanced warming and greening, this seasonal age polarization emerges earlier, persists longer, and becomes more pronounced, driving outflow and ET toward increasingly young water sources. This connectivity-driven tendency remains evident across variations in vegetation type, soil hydraulic properties, and slope gradient. Rather than progressively increasing groundwater dependence under drought, sustained hydrologic stress can suppress effective groundwater engagement, shorten hydrologic memory, and shift landscapes toward a shallower and faster mode of water cycling. Progressive groundwater decoupling therefore represents a structural transition in terrestrial water systems, with implications for predictability, resilience, and water resource stability under ongoing climate and vegetation change.

Deleted: stream

Deleted: strengthening

Deleted: buffering

Code and data availability

ParFlow version 3.14.1 was used in this study:
https://github.com/parflow/parflow/archive/refs/tags/v3.14.1.zip

EcoSLIM version 1.31 was employed for particle tracking:
https://github.com/reedmaxwell/EcoSLIM/archive/refs/tags/v1.31.zip

Minor modifications were made to the EcoSLIM source code to accommodate the experimental configuration described here.

All ParFlow and EcoSLIM run scripts for the full set of scenarios, together with the post-processing and figure-generation scripts, are available at https://doi.org/10.6084/m9.figshare.31410108

Author contribution

Conceptualization: CY. Methodology: CY and AS. Investigation: CY, AS, and WX. Resources: CY. Writing (original draft): CY, AS, and WX. Writing (review and editing): CY, AS, WX, EM, and HY.

Competing interests

The contact author has declared that none of the authors has any competing interests.

Supplementary Information

Text S1.

ParFlow (Kuffour et al., 2020; Maxwell, 2013; Kollet & Maxwell, 2006) solves variably saturated subsurface flow with the mixed form of Richards' equation and two-dimensional overland flow with the kinematic-wave approximation.

Richards' equation

$$S_s\, S(\psi)\, \frac{\partial \psi}{\partial t} + \phi\, \frac{\partial S(\psi)}{\partial t} = \nabla \cdot \boldsymbol{q} + q_s$$

$$\boldsymbol{q} = -\mathbf{K}_s\, k_r(\psi)\, \nabla(\psi - z)$$

where ψ is the pressure head $[L]$, $S(\psi)$ is the relative saturation, S_s is the specific storage coefficient $[L^{-1}]$, ϕ is porosity, $\boldsymbol{q}$ is the specific volumetric (Darcy) flux $[L\,T^{-1}]$, $\mathbf{K}_s$ is the saturated hydraulic conductivity tensor $[L\,T^{-1}]$, $k_r(\psi)$ is the relative permeability, z is depth below the surface [L], and q_s is a source/sink term $[T^{-1}]$. The non-linear relations $S(\psi)$ and $k_r(\psi)$ follow the van Genuchten-Mualem model.

Overland flow

$$\frac{\partial \psi_s}{\partial t} = \nabla \cdot (\mathbf{v}\, \psi_s) + q_r(x) + q_e(x)$$

with Manning's equation supplying the depth-averaged velocity components:

$$v_x = -\frac{\sqrt{S_{f,x}}}{n}\, \psi_s^{2/3}, \qquad v_y = -\frac{\sqrt{S_{f,y}}}{n}\, \psi_s^{2/3}$$

where ψ_s is the surface ponding depth $[L]$, $\mathbf{v} = (v_x, v_y)$ is the depth-averaged velocity $[L\,T^{-1}]$, q_r is the rainfall flux $[L\,T^{-1}]$, q_e is the subsurface-surface exchange flux $[L\,T^{-1}]$, $S_{f,i}$ is the friction slope (set equal to the bed slope under the kinematic-wave assumption), and n is Manning's roughness coefficient.

EcoSLIM (Maxwell et al., 2019; Yang et al., 2023) is an open-source Lagrangian particle-tracking model that calculates the advection and molecular diffusion of water parcels in the subsurface based on the transient three-dimensional velocity field generated by ParFlow-CLM. The position of a particle in the subsurface is described as (Tompson & Dougherty, 1988; Tompson & Gelhar, 1990):

$$\mathbf{S}(t + \Delta t) - \mathbf{S}(t) = \mathbf{A}\,\Delta t + \mathbf{B} \cdot \mathbf{Z}\sqrt{\Delta t}$$

$$\mathbf{A} \equiv \mathbf{v} + \nabla \cdot \mathbf{D} + \frac{\mathbf{D}}{\phi\,\theta} \cdot \nabla(\phi\,\theta)$$

$$\mathbf{B} \cdot \mathbf{B}^T \equiv 2\,\mathbf{D}$$

where $\mathbf{S}(t)$ is the position vector of the particle at time t $[L]$, Δt is the local timestep of the particle $[T]$, $\mathbf{Z}$ is a vector of pseudorandom numbers, $\mathbf{v}$ is the velocity vector at time t $[L\,T^{-1}]$, $\mathbf{D}$ is the

Formatted: Font: 13.5 pt

Formatted: Normal, Level 3, Space Before: Auto, After: Auto

Formatted: Font: Bold

Formatted: Justified

hydrodynamic dispersion tensor $[L^2\,T^{-1}]$, ϕ is the porosity, and θ is the saturation. The number density of particles $p(\mathbf{S},t)$ satisfies the Ito-Fokker-Planck approximation:

$$\frac{\partial p}{\partial t} + \nabla \cdot (\mathbf{A}\,p) - \Delta\left(\frac{1}{2}\,\mathbf{B} \cdot \mathbf{B}^T\,p\right) = 0$$

EcoSLIM determines the position of a water parcel by neglecting the macrodispersion in the equations above, yielding the advection-molecular-diffusion form actually solved in the code:

$$\mathbf{S}(t + \Delta t) - \mathbf{S}(t) = \mathbf{v}\,\Delta t + \mathbf{Z}\sqrt{2\,D_m\,\Delta t}$$

where D_m is the molecular diffusion coefficient $[L^2\,T^{-1}]$. Particles are dynamically added into the modeling domain where precipitation minus ET is positive (PME > 0). They move in the subsurface until they exit the domain as outflow (when they reach the stream bottom) or as ET (where PME < 0). Travel/residence times of outflow, ET, and groundwater are obtained by aggregating the travel times of the corresponding particles, and source composition is recovered by labeling particles with their water sources (e.g., snow, rainfall, or initial water).

References

Kollet, S.J., Maxwell, R.M. (2006). Integrated surface-groundwater flow modeling: A free-surface overland flow boundary condition in a parallel groundwater flow model. *Advances in Water Resources*, 29, 945-958.

Kuffour, B.N.O., et al. (2020). Simulating coupled surface-subsurface flows with ParFlow v3.5.0. *Geoscientific Model Development*, 13, 1373-1397.

Maxwell, R.M. (2013). A terrain-following grid transform and preconditioner for parallel, large-scale, integrated hydrologic modeling. *Advances in Water Resources*, 53, 109-117.

Maxwell, R.M., Condon, L.E., Danesh-Yazdi, M., Bearup, L.A. (2019). Exploring source water mixing and transient residence time distributions with EcoSLIM. *Ecohydrology*.

Tompson, A.F.B., Dougherty, D.E. (1988). On the use of particle tracking methods for solute transport in porous media. In *Computational Methods in Water Resources*, 2, 227-232.

Tompson, A.F.B., Gelhar, L.W. (1990). Numerical simulation of solute transport in three-dimensional, randomly heterogeneous porous media. *Water Resources Research*, 26(10), 2541-2562.

Yang, C., Ponder, C., Wang, B., Tran, H., Zhang, J., Swilley, J., Condon, L., Maxwell, R.M. (2023). Accelerating the Lagrangian particle tracking in hydrologic modeling to continental-scale. *Journal of Advances in Modeling Earth Systems*, 15, e2022MS003507.

Formatted: Justified, No bullets or numbering

Table S1. Maximum LAI values prescribed for the two vegetation types in the baseline, warming, greening, and warming–greening scenarios. All other vegetation parameters were kept at their default CLM settings.

Vegetation type	**Baseline**	**Warming**	**Greening**	**Warming+Greening**
Evergreen needleleaf forests	6	6	9	9
Open shrublands	6	6	9	9

Formatted: Font: (Default) Times New Roman

Formatted: Font: (Default) Times New Roman

Formatted: Font: (Default) Times New Roman

Figures S1–S10 correspond to the four forcing scenarios under the reference parameter set, whereas Figures S11–S16 present results from the three modified parameter sets.

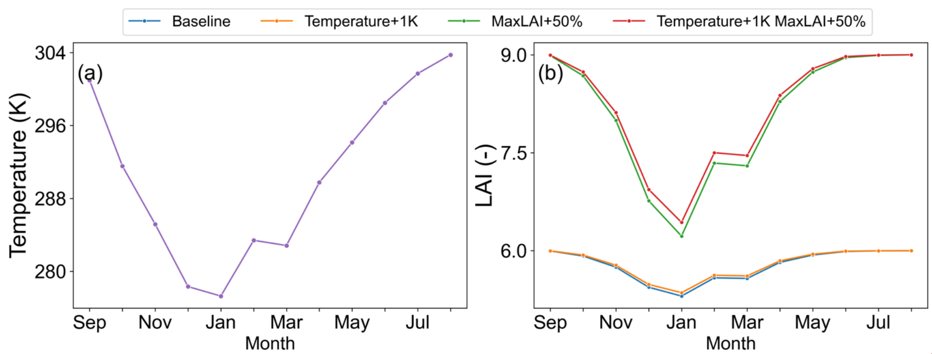

Figure S1. Monthly mean forcing conditions used in the four ET-forcing scenarios. (a) Air temperature and (b) leaf area index (LAI). The warming scenario increases air temperature uniformly by 1 °C throughout the year, while the greening scenario increases maximum LAI by 50%. The combined warming–greening scenario applies both perturbations simultaneously. Seasonal variations in temperature and vegetation activity are preserved across all scenarios, while the imposed perturbations enhance atmospheric and biological water demand.

Deleted: ¶

Deleted: ¶
Figure S1. Seasonal temperature (a) and LAI forcing across baseline and warming–greening scenarios (b)

Formatted: Font: Bold

Formatted: Justified

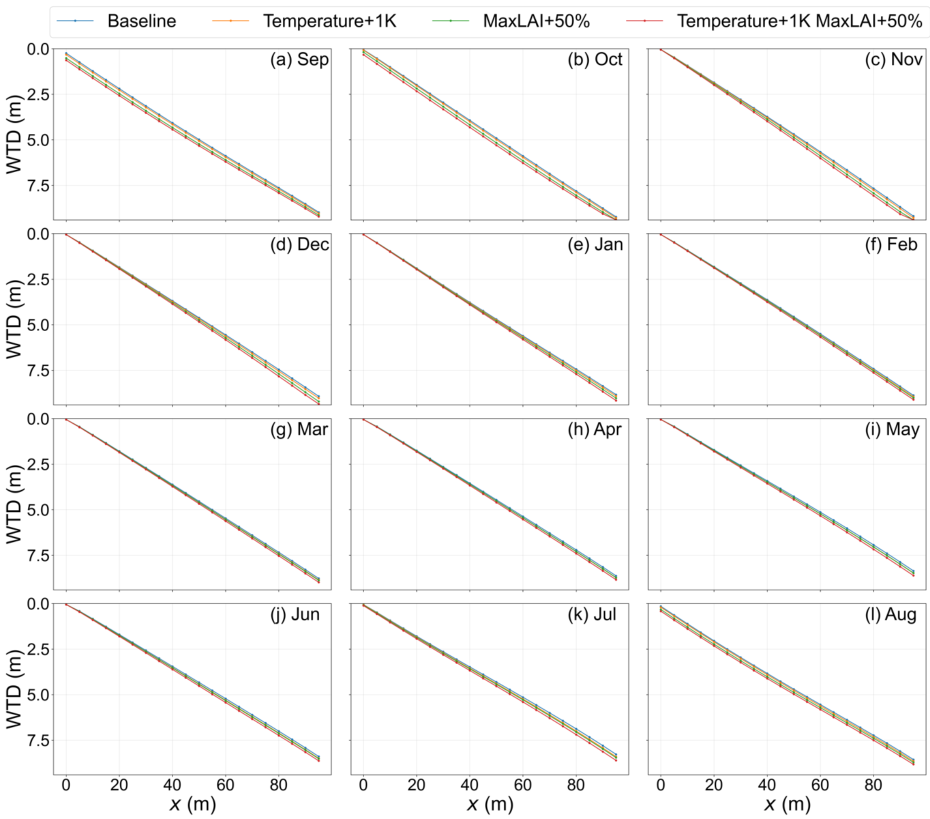

Figure S2. Seasonal evolution of water table depth (WTD) along the hillslope under the four ET-forcing scenarios. Enhanced ET forcing generally deepens the water table throughout the hillslope. In September, the water table near the hillslope outlet falls below the outlet elevation, indicating hydraulic disconnection between groundwater and the outlet. This disconnection coincides with the temporary loss of streamflow and the collapse of older-water contributions discussed in the main text.

Deleted: Figure S2. Seasonal evolution of water table depth along the hillslope under four forcing scenarios

Formatted: Font: Bold

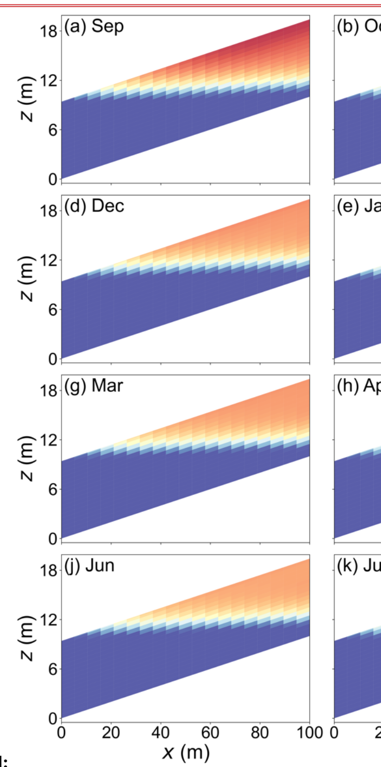

Deleted:

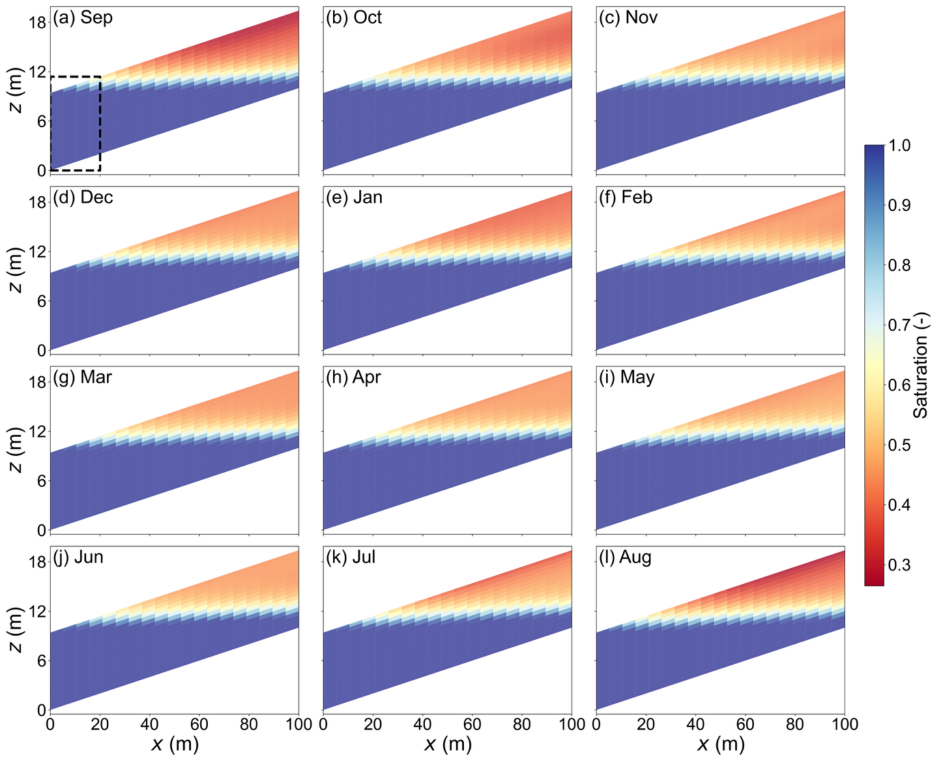

Figure S3. Seasonal evolution of hillslope saturation profiles under baseline conditions. Colors indicate saturation, with warmer colors representing drier conditions and cooler colors representing higher saturation. The dashed box highlights the lower 20 m section of the hillslope (x = 0–20 m) referred to in the main text. The saturation profiles show progressive drying and water-table decline during the late growing season (July–September), followed by gradual recovery during autumn, winter, and spring.

Deleted: **Figure S3. Seasonal evolution of hillslope saturation profiles**

Formatted: Justified

Deleted:

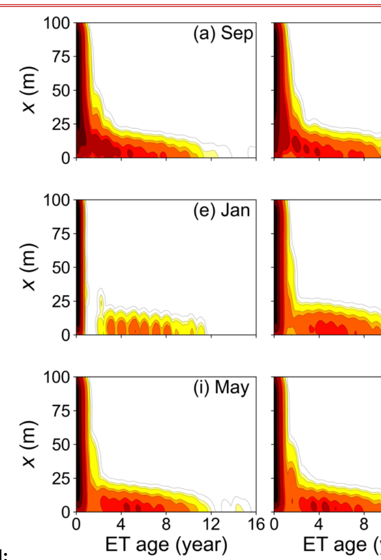

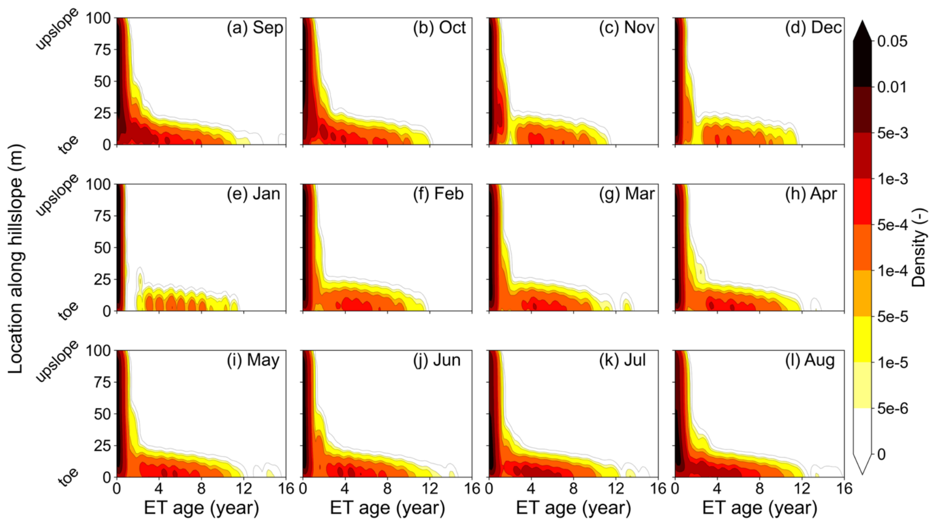

Figure S4. Seasonal evolution of ET age distributions along the hillslope under the warming scenario (+1 °C). Compared with the baseline case (Figure 4), warming promotes stronger depletion of intermediate-age contributions during winter and enhances the seasonal separation between younger and older ET age components.

Deleted: Figure S4. Seasonal evolution of ET age distributions under warming

Formatted: Font: Bold

Formatted: Justified

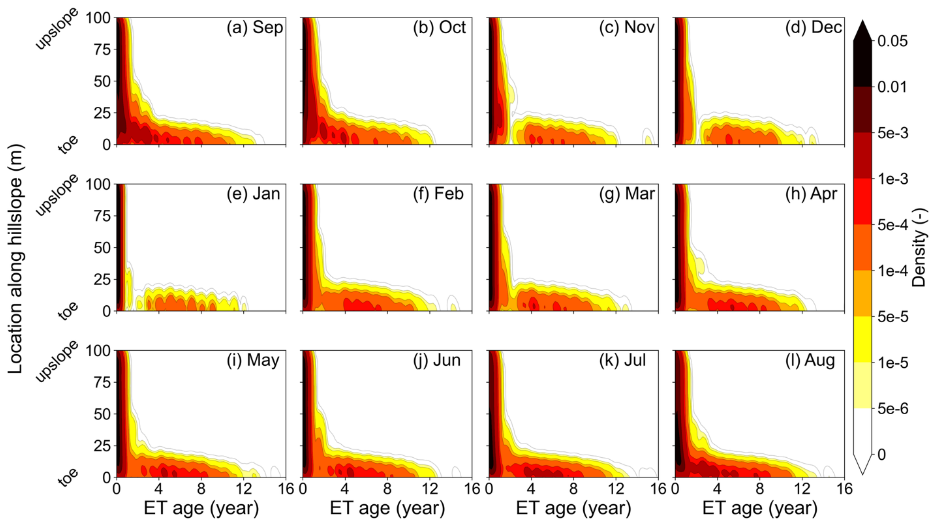

Figure S5. Seasonal evolution of ET age distributions along the hillslope under the greening scenario (MaxLAI +50%). Increased vegetation water demand enhances the depletion of intermediate-age contributions during winter, resulting in stronger seasonal age segregation compared with the baseline case (Figure 4).

Deleted:

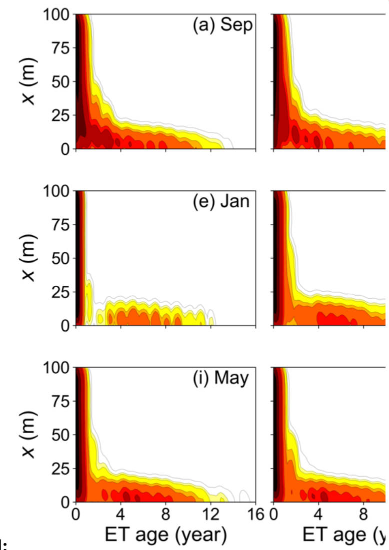

Deleted: Figure S5. Seasonal evolution of ET age distributions under greening

Formatted: Justified

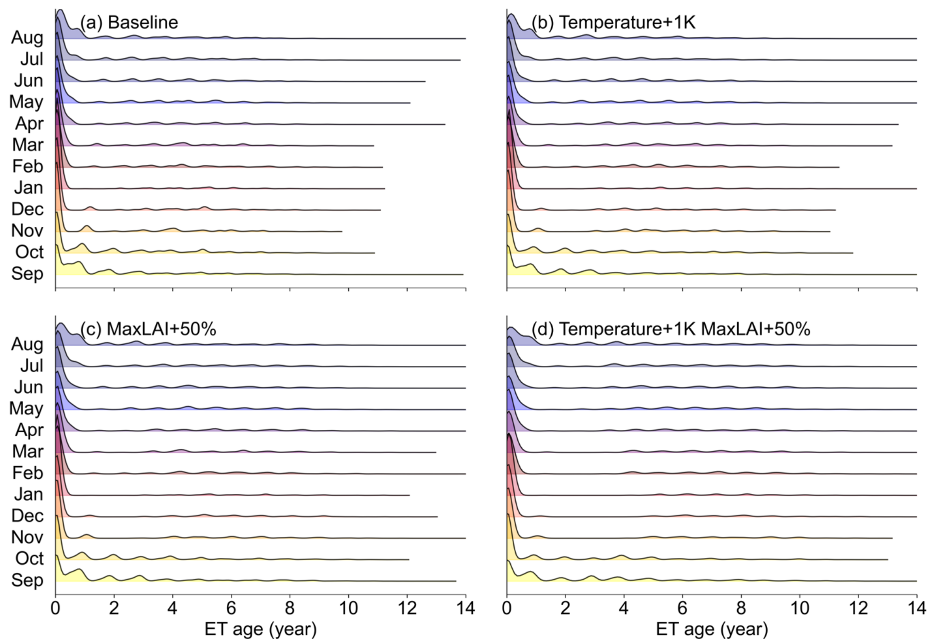

Figure S6. Seasonal ET age distributions within the lower 20 m section of the hillslope under the four ET-forcing scenarios. Compared with Figures 4, 5, S4, and S5, the spatial information is aggregated to highlight the age structure of ET source waters within the downslope zone. Despite the loss of spatial detail, the seasonal age gap remains clearly visible during winter (particularly in January), characterized by a marked depletion of intermediate-age contributions and only weak contributions from the oldest water components. Relative to the baseline case, enhanced ET forcing produces a wider age gap and stronger age polarization.

Deleted: Figure S6. Seasonal ET age distributions within the lower 20 m of the hillslope

Formatted: Font: Bold

Formatted: Justified

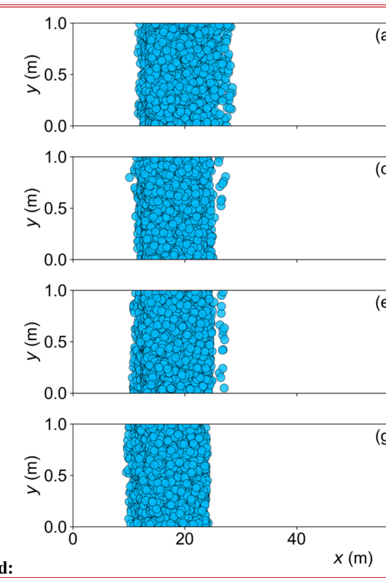

Deleted:

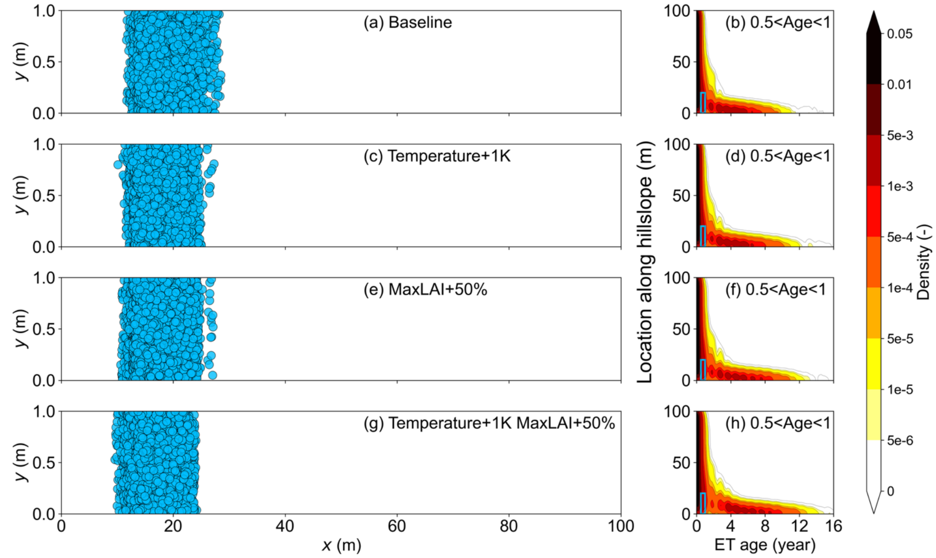

Figure S7. Source locations of ET particles with ages between 0.5 and 1 year contributing to annual ET within the downslope 20 m section of the hillslope under the four ET-forcing scenarios. Left panels show the inferred source locations of the selected particles in the x–y domain, while right panels show the corresponding ET age distributions as a function of distance along the hillslope. Blue rectangles indicate the selected age interval used to identify the particle populations shown in the left panels. Across all scenarios, these young ET particles originate predominantly from shallow and local source regions near the hillslope outlet, consistent with the dominance of rapidly recycled water in the young-age component.

Deleted: Figure S7. Source locations of ET particles (0.5–1 year) at the downslope 20 m section

Formatted: Font: Bold

Formatted: Font: Bold

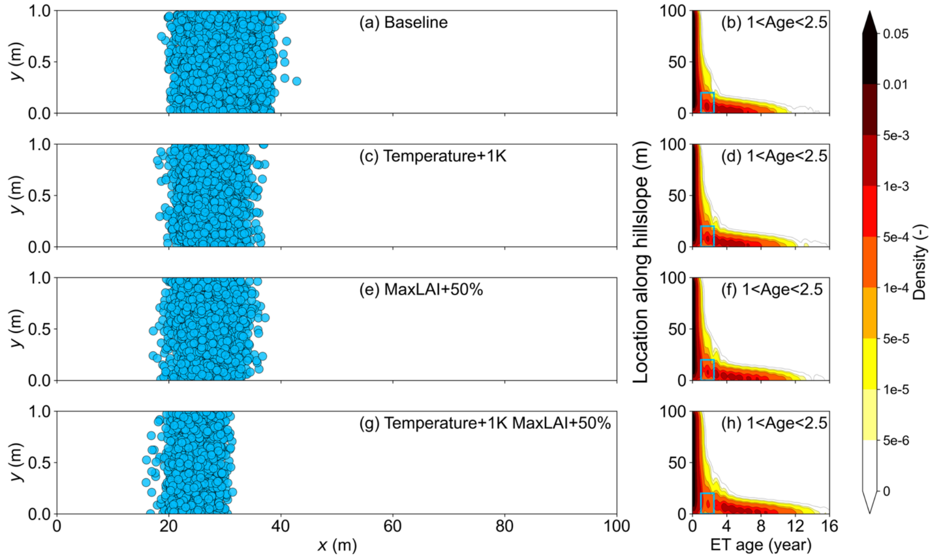

Figure S8. Source locations of ET particles with ages between 1 and 2.5 years contributing to annual ET within the downslope 20 m section of the hillslope under the four ET-forcing scenarios. Left panels show the inferred source locations of the selected particles in the x–y domain, while right panels show the corresponding ET age distributions as a function of distance along the hillslope. Blue rectangles indicate the selected age interval used to identify the particle populations shown in the left panels. Compared with the younger age class shown in Figure S7, these particles originate from more upslope locations, indicating that the older ET age component in the downslope zone is supplied by more distal subsurface storage rather than purely local recharge.

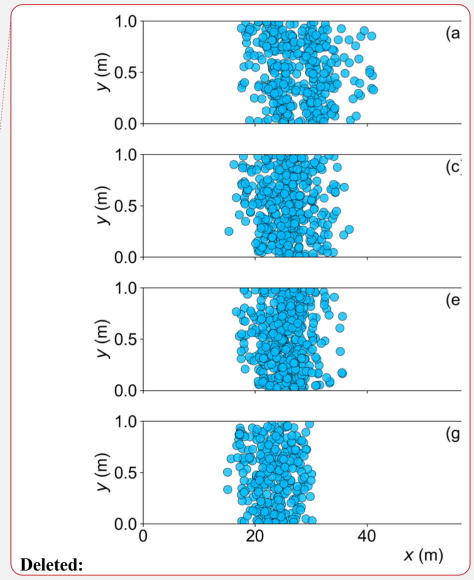

Deleted:

Deleted: ¶ ... [1]

Formatted: Font: Bold

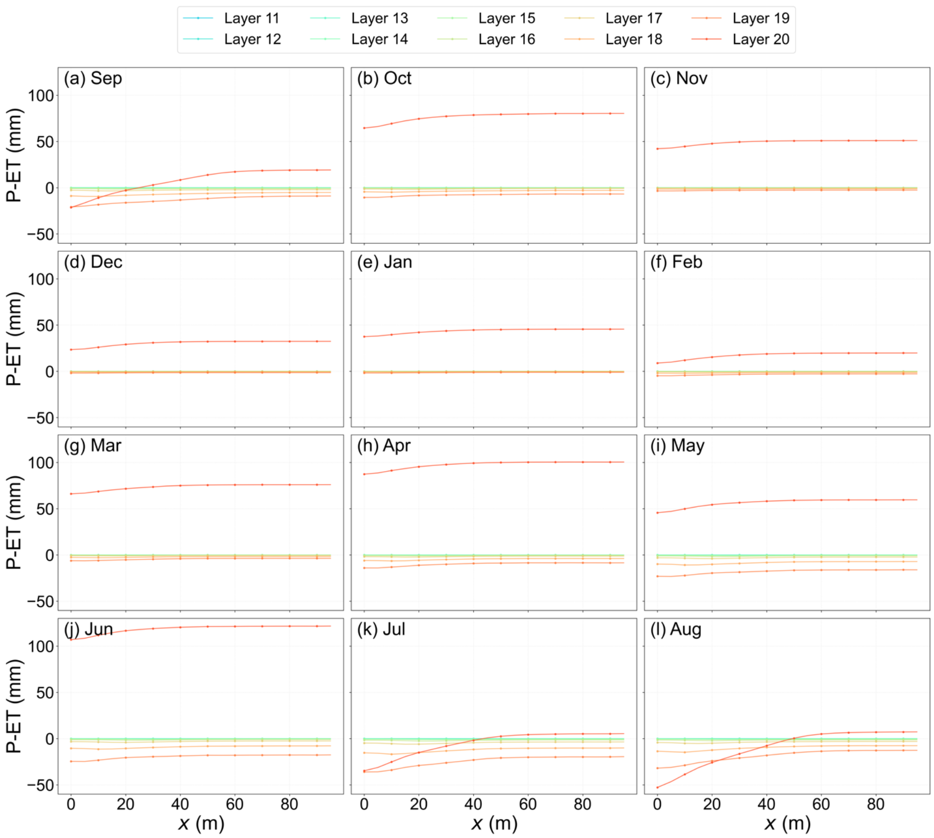

Figure S9. Monthly along-slope distribution of P–ET across root-zone layers under baseline forcing. Layers 11–20 are ordered from bottom to top within the root zone, with Layer 20 representing the uppermost root-zone layer. Positive values indicate net water gain (P > ET), whereas negative values indicate net water loss (ET > P). Most lower root-zone layers exhibit relatively small net fluxes throughout the year, while the uppermost root-zone layer (Layer 20) accounts for the majority of the seasonal water surplus and deficit. Positive P–ET during autumn, winter, and spring indicates recharge and storage recovery, whereas negative P–ET during late summer reflects enhanced water extraction and storage depletion.

Deleted: Figure S9. Monthly along-slope distribution of P–ET across root-zone layers under baseline forcing

Formatted: Font: Bold

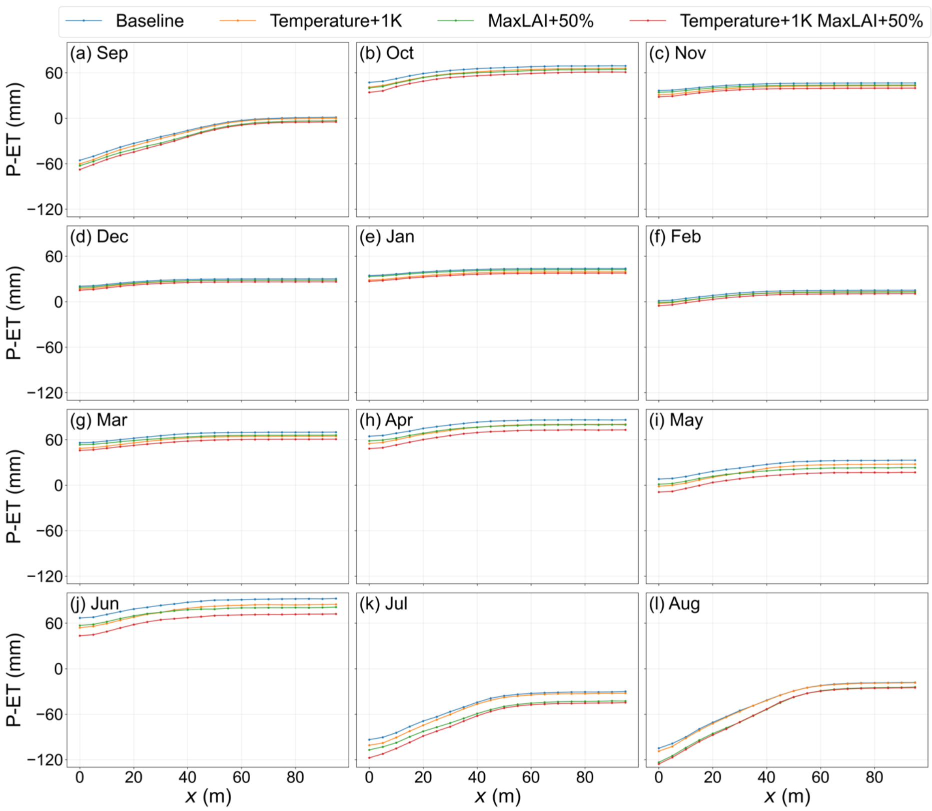

Figure S10. Monthly root-zone P–ET distribution along the hillslope under the four ET-forcing scenarios. Positive values indicate net water gain (P > ET), whereas negative values indicate net water loss (ET > P). The root zone experiences net recharge during autumn, winter, and spring and net water deficits during late summer. Enhanced ET forcing generally reduces recharge surpluses and intensifies summer deficits, indicating greater seasonal depletion of subsurface water storage under warming and greening conditions.

Deleted: Figure S10. Root-zone P–ET distribution along the hillslope under four scenarios

Formatted: Font: Bold

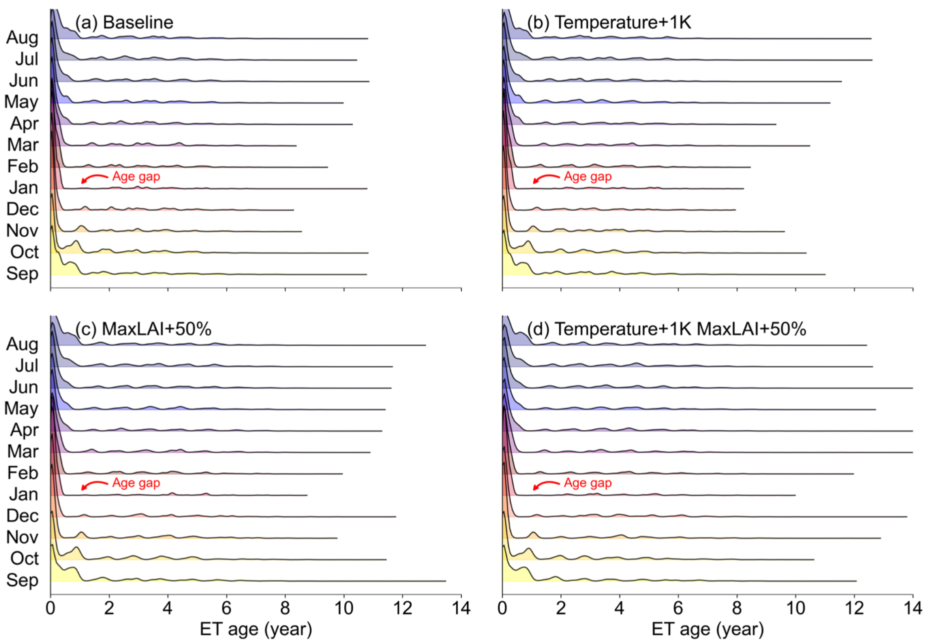

Figure S11. Seasonal ET age distributions within the lower 20 m section of the hillslope under shrub vegetation. Compared with the tree-covered reference configuration (Figure S6), reduced vegetation water demand weakens the seasonal depletion of intermediate-age contributions and results in a narrower age gap. Nevertheless, the age gap remains detectable during winter months, indicating that connectivity-driven age segregation persists despite reduced hydrologic stress.

Deleted: Figure S11. Seasonal ET age distributions within the lower 20 m of the hillslope under shrub vegetation

Formatted: Font: Bold

Formatted: Justified

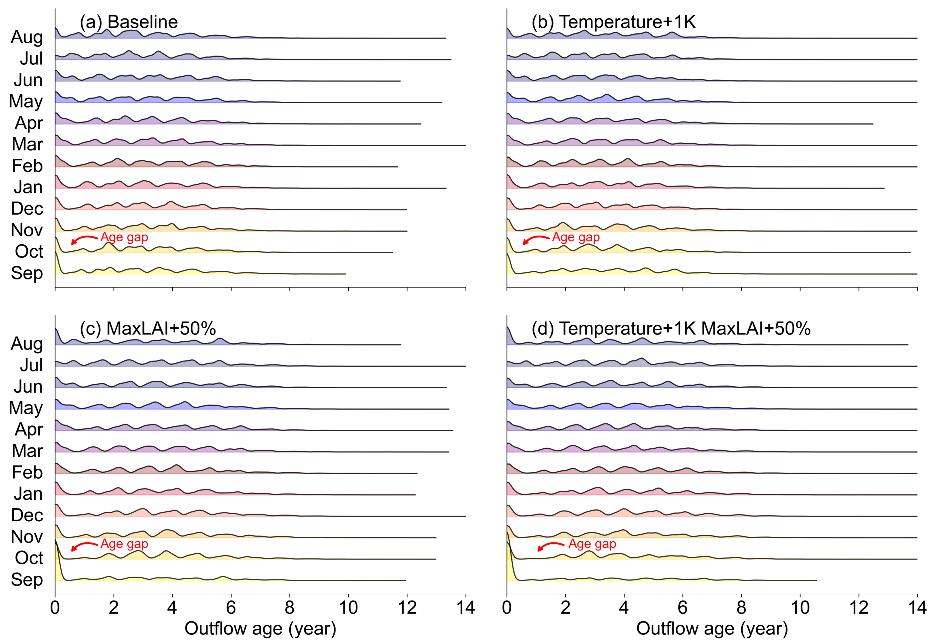

Figure S12. Seasonal outflow age distributions under shrub vegetation. Compared with the tree-covered reference configuration (Figure 6), reduced ET demand weakens seasonal age polarization and diminishes the magnitude of the age gap. However, the separation between younger and older outflow age components remains evident, demonstrating that the underlying reorganization tendency persists under lower vegetation water demand.

Deleted: Figure S12. Seasonal outflow age distributions within the lower 20 m of the hillslope under shrub vegetation

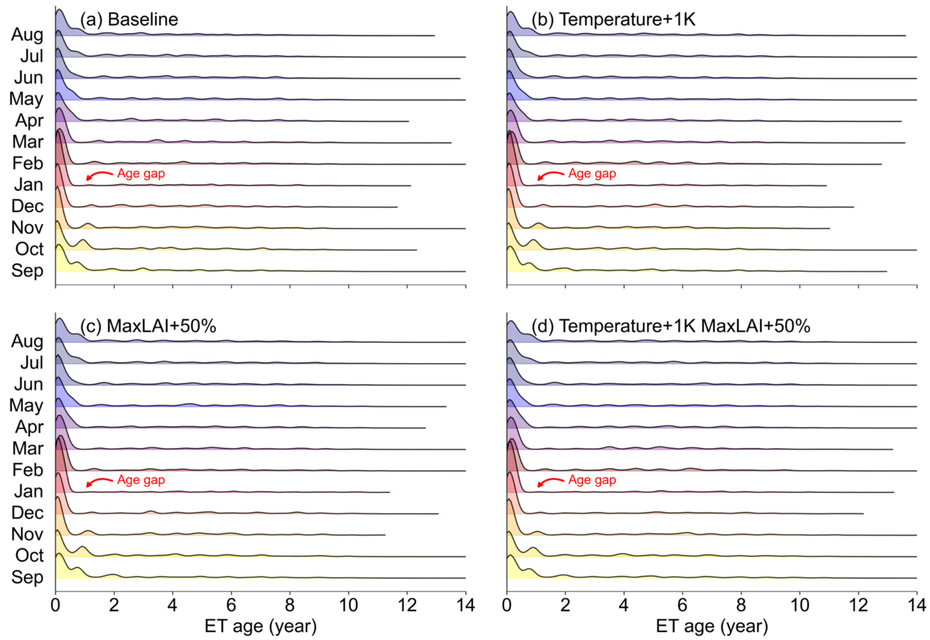

Figure S13. Seasonal ET age distributions within the lower 20 m section of the hillslope under modified subsurface hydraulic properties. Relative to the reference configuration (Figure S6), the modified hydraulic properties weaken the depletion of intermediate-age contributions and reduce the degree of age polarization. Although the age gap remains detectable during winter months, it is substantially muted, indicating that altered hydraulic properties redistribute ET contributions across age classes and weaken, but do not eliminate, the underlying age-segregation tendency.

Deleted: ¶ ... [2]

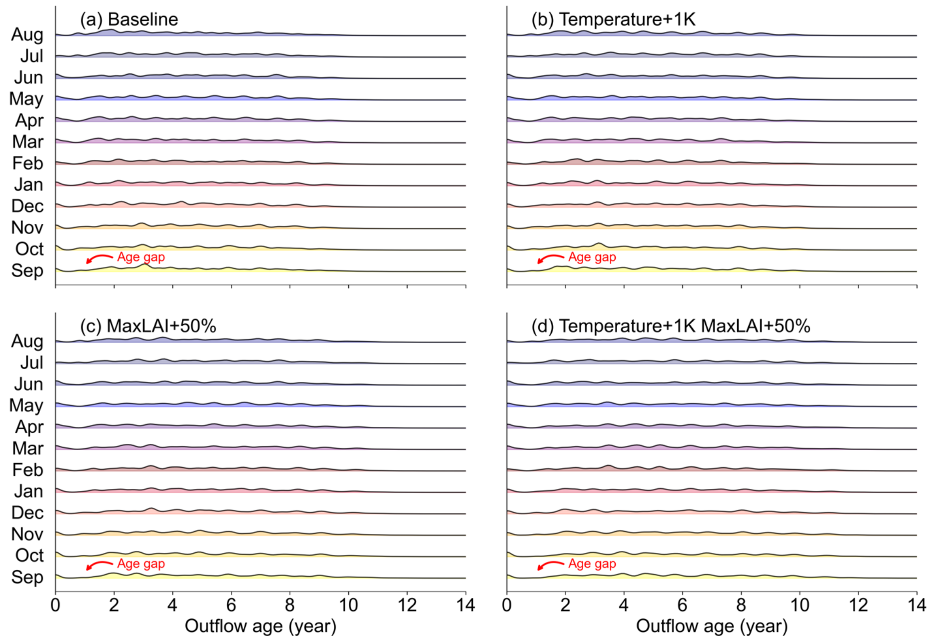

Figure S14. Seasonal outflow age distributions under modified subsurface hydraulic properties. Compared with the reference configuration (Figure 6), altered hydraulic properties increase the contribution of older water to outflow and weaken the seasonal age gap. The age gap remains identifiable but is considerably less pronounced, indicating that changes in hydraulic connectivity primarily redistribute the balance between young and old water contributions without eliminating the underlying age-segregation tendency.

Deleted: Figure S14. Seasonal outflow age distributions within the lower 20 m of the hillslope under modified subsurface hydraulic properties

Formatted: Font: Bold

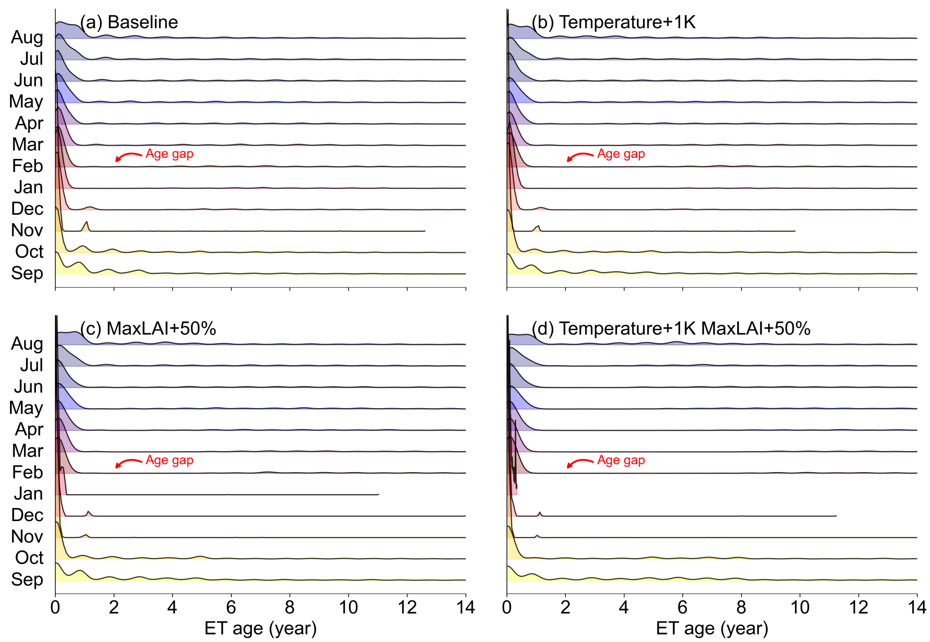

Figure S15. Seasonal ET age distributions within the lower 20 m section of the hillslope under reduced hillslope gradient. Relative to the reference configuration (Figure S6), weaker topographic control produces a substantially more pronounced age gap and stronger seasonal age segregation. During winter months, contributions from older ET water sources nearly disappear, leaving a clear separation between rapidly recycled young water and the remaining older age component. These patterns indicate enhanced seasonal decoupling under reduced hillslope gradient.

Deleted: Figure S15. Seasonal ET age distributions within the lower 20 m of the hillslope under reduced hillslope gradient

Formatted: Font: Bold

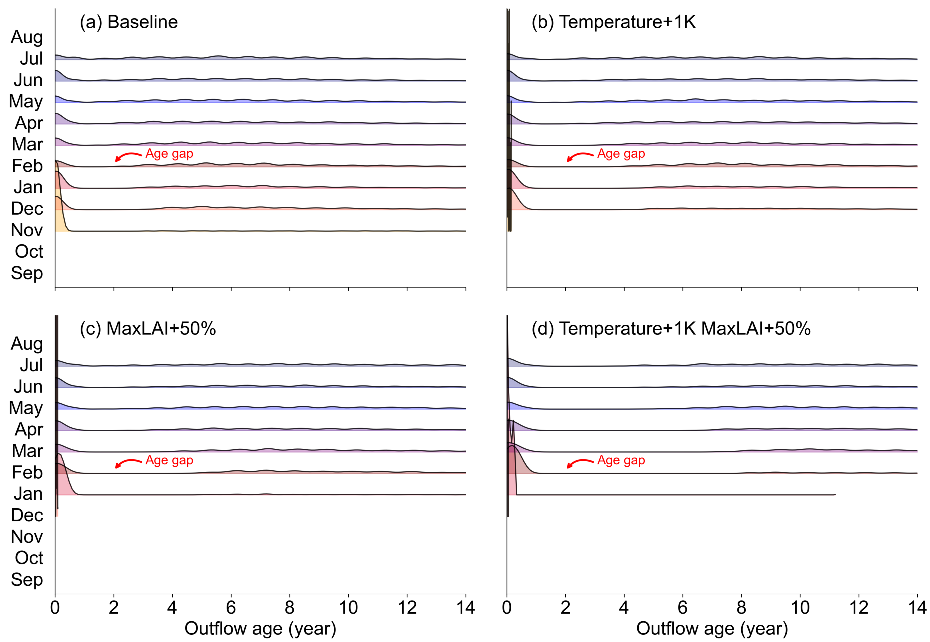

Figure S16. Seasonal outflow age distributions under reduced hillslope gradient. Compared with the reference configuration (Figure 6), reduced hillslope gradient strongly suppresses older-water contributions during winter months and produces a wider and more persistent age gap. The resulting age distributions are dominated by young water, indicating enhanced groundwater–surface decoupling and weaker hydraulic connectivity under reduced topographic forcing.

Deleted: Figure S16. Seasonal outflow age distributions within the lower 20 m of the hillslope under reduced hillslope gradient

Formatted: Font: Bold

References

Bearup, L. A., Maxwell, R. M., & McCray, J. E. (2016). Hillslope response to insect-induced land-cover change: an integrated model of end-member mixing. *Ecohydrology*, *9*(2), 195-203. <Go to ISI>://WOS:000372309400001

Berkowitz, B., & Zehe, E. (2020). Surface water and groundwater: unifying conceptualization and quantification of the two "water worlds". *Hydrol. Earth Syst. Sci.*, *24*(4), 1831-1858. https://doi.org/10.5194/hess-24-1831-2020

Betterle, A., & Bellin, A. (2024). Morphological and Hydrogeological Controls of Groundwater Flows and Water Age Distribution in Mountain Aquifers and Streams. *Water Resources Research*, *60*(11), e2024WR037407. https://doi.org/https://doi.org/10.1029/2024WR037407

Bierkens, M. F. P., & van den Hurk, B. J. J. M. (2007). Groundwater convergence as a possible mechanism for multi-year persistence in rainfall. *Geophysical Research Letters*, *34*(2). https://doi.org/10.1029/2006GL028396

Brooks, P. D., Gelderloos, A., Wolf, M. A., Jamison, L. R., Strong, C., Solomon, D. K., Bowen, G. J., Burian, S., Tai, X., Arens, S., Briefer, L., Kirkham, T., & Stewart, J. (2021). Groundwater-Mediated Memory of Past Climate Controls Water Yield in Snowmelt-Dominated Catchments. *Water Resources Research*, *57*(10), e2021WR030605. https://doi.org/https://doi.org/10.1029/2021WR030605

Carroll, R. W. H., Niswonger, R. G., Ulrich, C., Varadharajan, C., Siirila-Woodburn, E. R., & Williams, K. H. (2024). Declining groundwater storage expected to amplify mountain streamflow reductions in a warmer world. *Nature Water*, *2*(5), 419-433. https://doi.org/10.1038/s44221-024-00239-0

Chen, C., Park, T., Wang, X., Piao, S., Xu, B., Chaturvedi, R. K., Fuchs, R., Brovkin, V., Ciais, P., Fensholt, R., Tømmervik, H., Bala, G., Zhu, Z., Nemani, R. R., & Myneni, R. B. (2019). China and India lead in greening of the world through land-use management. *Nature Sustainability*, *2*(2), 122-129. https://doi.org/10.1038/s41893-019-0220-7

Condon, L. E., Atchley, A. L., & Maxwell, R. M. (2020). Evapotranspiration depletes groundwater under warming over the contiguous United States. *Nature Communications*, *11*(1), 873. https://doi.org/10.1038/s41467-020-14688-0

Danesh-Yazdi, M., Klaus, J., Condon, L. E., & Maxwell, R. M. (2018). Bridging the gap between numerical solutions of travel time distributions and analytical storage selection functions. *Hydrological Processes*, *32*(8), 1063-1076. <Go to ISI>://WOS:000430466700006

Elsaidy, A., Yimer, E. A., Mogheir, Y., Huysmans, M., Villani, L., & van Griensven, A. (2025). Groundwater drought and anthropogenic amplifiers: A review of assessment and response strategies in arid and semi-arid areas. *Science of the Total Environment*, *978*, 179406. https://doi.org/https://doi.org/10.1016/j.scitotenv.2025.179406

Fan, Y., Clark, M., Lawrence, D. M., Swenson, S., Band, L. E., Brantley, S. L., Brooks, P. D., Dietrich, W. E., Flores, A., Grant, G., Kirchner, J. W., Mackay, D. S., McDonnell, J. J., Milly, P. C. D., Sullivan, P. L., Tague, C., Ajami, H., Chaney, N., Hartmann, A.,...Yamazaki, D. (2019). Hillslope Hydrology in Global Change Research and Earth

System Modeling. *Water Resources Research*, *55*(2), 1737-1772. https://doi.org/10.1029/2018wr023903

Fan, Y., Miguez-Macho, G., Jobbágy, E. G., Jackson, R. B., & Otero-Casal, C. (2017). Hydrologic regulation of plant rooting depth. *Proceedings of the National Academy of Sciences*, *114*(40), 10572-10577. https://doi.org/10.1073/pnas.1712381114

Floriancic, M. G., Allen, S. T., & Kirchner, J. W. (2024). Young and new water fractions in soil and hillslope waters. *Hydrol. Earth Syst. Sci.*, *28*(18), 4295-4308. https://doi.org/10.5194/hess-28-4295-2024

Getirana, A., Kumar, S., & Rodell, M. (2025). Inconsistencies in GRACE-Based Groundwater Storage Estimation—A Call for a Proper Use of Land Surface Models. *Geophysical Research Letters*, *52*(19), e2025GL119197. https://doi.org/https://doi.org/10.1029/2025GL119197

Ipcc. (2021). *Climate Change 2021: The Physical Science Basis. Contribution of Working Group I to the Sixth Assessment Report of the Intergovernmental Panel on Climate Change* (Vol. In Press). Cambridge University Press. https://doi.org/10.1017/9781009157896

Jasechko, S., Seybold, H., Perrone, D., Fan, Y., Shamsudduha, M., Taylor, R. G., Fallatah, O., & Kirchner, J. W. (2024). Rapid groundwater decline and some cases of recovery in aquifers globally. *Nature*, *625*(7996), 715-721. https://doi.org/10.1038/s41586-023-06879-8

Jencso, K. G., McGlynn, B. L., Gooseff, M. N., Wondzell, S. M., Bencala, K. E., & Marshall, L. A. (2009). Hydrologic connectivity between landscapes and streams: Transferring reach- and plot-scale understanding to the catchment scale. *Water Resources Research*, *45*(4). https://doi.org/https://doi.org/10.1029/2008WR007225

Knighton, J., & Berghuijs, W. R. (2023). Water Ages Explain Tradeoffs Between Long-Term Evapotranspiration and Ecosystem Drought Resilience. *Geophysical Research Letters*, *50*(10), e2023GL103649. https://doi.org/https://doi.org/10.1029/2023GL103649

Kollet, S. J., & Maxwell, R. M. (2006). Integrated surface-groundwater flow modeling: A free-surface overland flow boundary condition in a parallel groundwater flow model. *Advances in Water Resources*, *29*(7), 945-958. <Go to ISI>://WOS:000238830800001

Kollet, S. J., & Maxwell, R. M. (2008). Capturing the influence of groundwater dynamics on land surface processes using an integrated, distributed watershed model. *Water Resources Research*, *44*(2). https://doi.org/Artn W02402

10.1029/2007wr006004

Li, L., Knapp, J. L. A., Lintern, A., Ng, G. H. C., Perdrial, J., Sullivan, P. L., & Zhi, W. (2024). River water quality shaped by land–river connectivity in a changing climate. *Nature Climate Change*, *14*(3), 225-237. https://doi.org/10.1038/s41558-023-01923-x

Liang, X., Schilling, K. E., Jones, C. S., & Zhang, Y.-K. (2021). Temporal scaling of long-term co-occurring agricultural contaminants and the implications for conservation planning. *Environmental Research Letters*, *16*(9), 094015. https://doi.org/10.1088/1748-9326/ac19dd

Maxwell, R. M. (2013). A terrain-following grid transform and preconditioner for parallel, large-scale, integrated hydrologic modeling. *Advances in Water Resources*, *53*, 109-117. https://doi.org/https://doi.org/10.1016/j.advwatres.2012.10.001

Maxwell, R. M., Condon, L. E., Danesh-Yazdi, M., & Bearup, L. A. (2019). Exploring source water mixing and transient residence time distributions of outflow and evapotranspiration with an integrated hydrologic model and Lagrangian particle tracking approach. *Ecohydrology*, *12*(1). <Go to ISI>://WOS:000454601400016

Maxwell, R. M., & Miller, N. L. (2005). Development of a coupled land surface and groundwater model. *Journal of Hydrometeorology*, *6*(3), 233-247. <Go to ISI>://WOS:000230393600001

Miguez-Macho, G., & Fan, Y. (2021). Spatiotemporal origin of soil water taken up by vegetation. *Nature*, *598*(7882), 624-628. https://doi.org/10.1038/s41586-021-03958-6

Miguez-Macho, G., & Fan, Y. (2025). A global humidity index with lateral hydrologic flows. *Nature*, *644*(8076), 413-419. https://doi.org/10.1038/s41586-025-09359-3

Mikkelson, K. M., Maxwell, R. M., Ferguson, I., Stednick, J. D., McCray, J. E., & Sharp, J. O. (2013). Mountain pine beetle infestation impacts: modeling water and energy budgets at the hill-slope scale. *Ecohydrology*, *6*(1), 64-72. https://doi.org/https://doi.org/10.1002/eco.278

Piao, S. L., Wang, X. H., Park, T., Chen, C., Lian, X., He, Y., Bjerke, J. W., Chen, A. P., Ciais, P., Tommervik, H., Nemani, R. R., & Myneni, R. B. (2020). Characteristics, drivers and feedbacks of global greening. *Nature Reviews Earth & Environment*, *1*(1), 14-27. https://doi.org/10.1038/s43017-019-0001-x

Pokhrel, Y., Felfelani, F., Satoh, Y., Boulange, J., Burek, P., Gädeke, A., Gerten, D., Gosling, S. N., Grillakis, M., Gudmundsson, L., Hanasaki, N., Kim, H., Koutroulis, A., Liu, J., Papadimitriou, L., Schewe, J., Müller Schmied, H., Stacke, T., Telteu, C.-E.,...Wada, Y. (2021). Global terrestrial water storage and drought severity under climate change. *Nature Climate Change*, *11*(3), 226-233. https://doi.org/10.1038/s41558-020-00972-w

Schiavo, M., Riva, M., Guadagnini, L., Zehe, E., & Guadagnini, A. (2022). Probabilistic identification of Preferential Groundwater Networks. *Journal of Hydrology*, *610*, 127906. https://doi.org/https://doi.org/10.1016/j.jhydrol.2022.127906

Seager, R., Feldman, J., Lis, N., Ting, M., Williams, A. P., Nakamura, J., Liu, H., & Henderson, N. (2018). Whither the 100th Meridian? The Once and Future Physical and Human Geography of America's Arid–Humid Divide. Part II: The Meridian Moves East. *Earth Interactions*, *22*(5), 1-24. https://doi.org/https://doi.org/10.1175/EI-D-17-0012.1

Seager, R., Lis, N., Feldman, J., Ting, M., Williams, A. P., Nakamura, J., Liu, H., & Henderson, N. (2018). Whither the 100th Meridian? The Once and Future Physical and Human Geography of America's Arid–Humid Divide. Part I: The Story So Far. *Earth Interactions*, *22*(5), 1-22. https://doi.org/https://doi.org/10.1175/EI-D-17-0011.1

Shi, H., Jin, F.-F., Wills, R. C. J., Jacox, M. G., Amaya, D. J., Black, B. A., Rykaczewski, R. R., Bograd, S. J., García-Reyes, M., & Sydeman, W. J. (2022). Global decline in ocean memory over the 21st century. *Science Advances*, *8*(18), eabm3468. https://doi.org/doi:10.1126/sciadv.abm3468

Somers, L. D., & McKenzie, J. M. (2020). A review of groundwater in high mountain environments. *WIREs Water*, *7*(6), e1475. https://doi.org/https://doi.org/10.1002/wat2.1475

Swenson, L. J., Zipper, S., Peterson, D. M., Jones, C. N., Burgin, A. J., Seybold, E., Kirk, M. F., & Hatley, C. (2024). Changes in Water Age During Dry-Down of a Non-Perennial Stream. *Water Resources Research*, *60*(1), e2023WR034623. https://doi.org/https://doi.org/10.1029/2023WR034623

Tan, X., Liu, B., & Tan, X. (2020). Global Changes in Baseflow Under the Impacts of Changing Climate and Vegetation. *Water Resources Research*, *56*(9), e2020WR027349. https://doi.org/https://doi.org/10.1029/2020WR027349

Tran, H., Zhang, J., Cohard, J.-M., Condon, L. E., & Maxwell, R. M. (2020). Simulating Groundwater-Streamflow Connections in the Upper Colorado River Basin. *Groundwater*, *58*(3), 392-405. https://doi.org/10.1111/gwat.13000

Villaruel, A. J., Seck, A., & Schultz, C. (2025). Evaluating time-lagged relationships between groundwater storage and river discharge using GRACE-based data: insights from the Potomac Basin. *Environmental Research Communications*, *7*(7), 075003. https://doi.org/10.1088/2515-7620/ade36f

Visser, A., Thaw, M., Deinhart, A., Bibby, R., Safeeq, M., Conklin, M., Esser, B., & Van der Velde, Y. (2019). Cosmogenic Isotopes Unravel the Hydrochronology and Water Storage Dynamics of the Southern Sierra Critical Zone. *Water Resources Research*, *55*(2), 1429-1450. https://doi.org/https://doi.org/10.1029/2018WR023665

von Freyberg, J., Allen, S. T., Seeger, S., Weiler, M., & Kirchner, J. W. (2018). Sensitivity of young water fractions to hydro-climatic forcing and landscape properties across 22 Swiss catchments. *Hydrol. Earth Syst. Sci.*, *22*(7), 3841-3861. https://doi.org/10.5194/hess-22-3841-2018

Wilusz, D. C., Harman, C. J., Ball, W. B., Maxwell, R. M., & Buda, A. R. (2019). Using particle tracking to understand flow paths, age distributions, and the paradoxical origins of the inverse storage effect in an experimental catchment. *Water Resources Research*, *n/a*(n/a), e24397. https://doi.org/10.1029/2019wr025140

Xie, J., Liu, X., Jasechko, S., Berghuijs, W. R., Wang, K., Liu, C., Reichstein, M., Jung, M., & Koirala, S. (2024). Majority of global river flow sustained by groundwater. *Nature Geoscience*, *17*(8), 770-777. https://doi.org/10.1038/s41561-024-01483-5

Yang, C., Maxwell, R., McDonnell, J., Yang, X., & Tijerina-Kreuzer, D. (2023). The Role of Topography in Controlling Evapotranspiration Age. *Journal of Geophysical Research: Atmospheres*, *128*(18), e2023JD039228. https://doi.org/https://doi.org/10.1029/2023JD039228

Yang, C., Maxwell, R. M., & Valent, R. (2022). Accelerating the Lagrangian simulation of water ages on distributed, multi-GPU platforms: The importance of dynamic load balancing. *Computers & Geosciences*, *166*, 105189. https://doi.org/https://doi.org/10.1016/j.cageo.2022.105189

Yang, C., Zhang, Y. K., Liang, X. Y., Olschanowsky, C., Yang, X. F., & Maxwell, R. (2021). Accelerating the Lagrangian particle tracking of residence time distributions and source water mixing towards large scales. *Computers & Geosciences*, *151*. <Go to ISI>://WOS:000641463100004

Yang, X., Tetzlaff, D., Soulsby, C., Smith, A., & Borchardt, D. (2021). Catchment Functioning Under Prolonged Drought Stress: Tracer-Aided Ecohydrological Modeling in an Intensively Managed Agricultural Catchment. *Water Resources Research*, *57*(3), e2020WR029094. https://doi.org/https://doi.org/10.1029/2020WR029094

Yang, Y., Roderick, M. L., Guo, H., Miralles, D. G., Zhang, L., Fatichi, S., Luo, X., Zhang, Y., McVicar, T. R., Tu, Z., Keenan, T. F., Fisher, J. B., Gan, R., Zhang, X., Piao, S., Zhang, B., & Yang, D. (2023). Evapotranspiration on a greening Earth. *Nature Reviews Earth & Environment*, *4*(9), 626-641. https://doi.org/10.1038/s43017-023-00464-3

Zipper, S., Brookfield, A., Ajami, H., Ayers, J. R., Beightel, C., Fienen, M. N., Gleeson, T., Hammond, J., Hill, M., Kendall, A. D., Kerr, B., Lapides, D., Porter, M., Parimalarenganayaki, S., Rohde, M. M., & Wardropper, C. (2024). Streamflow Depletion Caused by Groundwater Pumping: Fundamental Research Priorities for Management-Relevant Science. *Water Resources Research*, *60*(5), e2023WR035727. https://doi.org/https://doi.org/10.1029/2023WR035727

Page 27: [1] Deleted	Chen Yang	6/16/26 11:17:00 AM

Page 32: [2] Deleted	Chen Yang	6/5/26 7:49:00 PM